ELSEVIER

Physica D 129 (1999) 171–202

PHYSICA D

Takens–Bogdanov bifurcation on the hexagonal lattice for double-layer convection

Yuriko Yamamuro Renardy [a,*], Michael Renardy [b], Kaoru Fujimura[c,1]

[a] *Department of Mathematics and Interdisciplinary Center for Mathematics, Virginia Polytechnic Institute and State University, Blacksburg, VA 24061-0123, USA*

[b] *Department of Mathematics and ICAM, V.P.I & S.U., Blacksburg, VA 24061-0123, USA*

[c] *Japan Atomic Energy Research Institute, Tokai-mura, Ibaraki 319-11, Japan*

Received 20 April 1998; received in revised form 10 December 1998; accepted 7 January 1999
Communicated by F. H. Busse

Abstract

In the Bénard problem for two-fluid layers, Takens–Bogdanov bifurcations can arise when the stability thresholds for both layers are close to each other. In this paper, we provide an analysis of bifurcating solutions near such a Takens–Bogdanov point, under the assumption that solutions are doubly periodic with respect to a hexagonal lattice. Our analysis focusses on periodic solutions, secondary bifurcations from steady to periodic solutions and heteroclinic solutions arising as limits of periodic solutions. We compute the coefficients of the amplitude equations for a number of physical situations. Numerical integration of the amplitude equations reveals quasiperiodic and chaotic regimes, in addition to parameter regions where steady or periodic solutions are observed.

1. Introduction

The two-layer Bénard problem concerns instabilities that arise when a two-layer system is heated from below. An instability may take place when the temperature difference between the upper and lower walls reaches a threshold value, or it may take place even at very low Rayleigh numbers due to the stratification in the fluid properties. A time-periodic onset of instability is possible, and there are two very distinct mechanisms involved. Each mechanism consists of two modes competing with each other to set up the oscillations. The first is associated with a deformable interface, and the oscillations are due to the competition between the Bénard instability (due to a bulk mode destabilization) and a stabilizing interface (due to an appropriate stratification in fluid properties). The eigenmodes consist of time-periodic convection cells which extend through both fluids. This mechanism was studied in [1,2].

* Corresponding author. Tel.: +1-540-231-8258; fax: +1-540-231-5960; e-mail: renardyy@math.vt.edu.
[1] Permanent address. Department of Applied Mathematics and Physics, Tottori University, Tottori 680, Japan.

0167-2789/99/$ – see front matter
PII: S0167-2789(99)00007-X

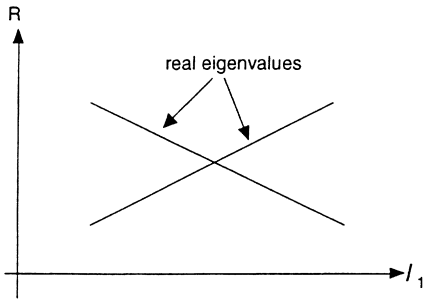

Fig. 1. Sketch of cross-over of eigenvalues for a degenerate double zero eigenvalue over a range of bifurcation parameters, R and l_1 to be defined later as the Rayleigh number and the dimensionless depth of the lower liquid.

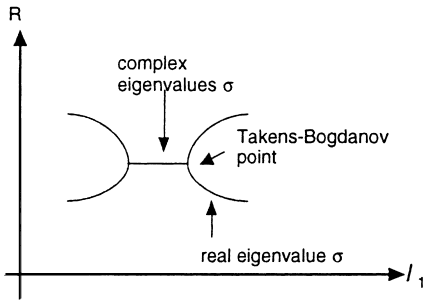

Fig. 2. Sketch showing cross-over of real eigenvalues to form complex conjugates at two Takens–Bogdanov points.

A second mechanism for oscillatory onset arises when interface deformation is negligible. In this case, the critical eigenmode consists of two cells arranged one above the other, that is, one in each fluid [3–6]. This mechanism has recently drawn the interest from experimental physicists [7,8,24]. Oscillatory onset can occur if the effective Rayleigh numbers for each layer are roughly equal. The fact that a criterion of nearly equal Rayleigh numbers applies suggests that the occurrence of complex eigenvalues can be thought of as resulting from the near crossover of two real eigenvalues. Indeed, there are special values for the ratios of fluid properties for which the problem is self-adjoint, so real eigenvalues would then cross without becoming complex. This observation has led to studies of bifurcations in the neighborhood of a double zero eigenvalue which represents such a crossover [9,10]. Fig. 1 is a sketch of the situation for the two-layer problem, with the vertical axis representing a parameter such as the Rayleigh number, and the horizontal axis representing another parameter, such as the dimensionless depth of the lower liquid. In this paper, we focus on a less degenerate situation, which is that of a Takens–Bogdanov point. Fig. 2 is a sketch of this in terms of the relevant parameters for the two-layer problem, analogous to Fig. 1. Such a point represents the merger of two real eigenvalues which then form a complex conjugate pair. This is less degenerate than the crossover of two real eigenvalues, which can be thought of as arising from the merger of two Takens–Bogdanov points. Since the window for the complex eigenvalues in Fig. 2 is small, this picture may be thought of as a perturbation of the situation in Fig. 1.

Takens–Bogdanov bifurcations without symmetries or with simple symmetries such as Z_2 or O(2) are well-studied and much is known about periodic and homoclinic solutions [11–14]. However, the case of the hexagonal lattice, which is of interest for the Bénard problem, remains to be investigated.

Below, we discuss how to derive the amplitude equations governing the neighborhood of a Takens–Bogdanov point, and how to obtain them by a limiting procedure when the frequency of a Hopf bifurcation tends to zero. We then analyze the existence of bifurcating solutions of various symmetry classes. For the case of Hopf bifurcation,

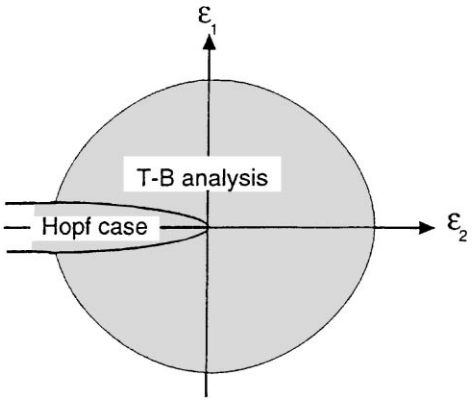

Fig. 3. Sketch of the region of validity of the analysis carried out in this paper in $\epsilon_1 - \epsilon_2$ plane, where the bifurcation parameters are defined in Section 5. The analysis for the Hopf case, with small frequencies, is limited to the region close to the ϵ_2 axis as shown.

periodic solutions which have 'maximal' symmetry were classified by Roberts, Swift and Wagner [15]. In the Takens–Bogdanov case, we recover the same types of periodic solutions, but some of them can now also arise as a secondary bifurcation from steady solutions rather than as a bifurcation directly from the rest state. In some cases, we can also establish the existence of homoclinic or heteroclinic orbits which arise as limits of periodic solutions. The aim of this bifurcation analysis is to provide solutions that are valid far enough from the point of onset to be applicable to experiments. Recall that the analysis for the Hopf bifurcation case [5] is based on assuming a nonzero frequency, and as the frequency tends to zero, the region of validity of the analysis shrinks. Hopf bifurcations close to a Takens–Bogdanov point involve eigenvalues with small frequencies, which limits the region of validity of the theory in Fig. 3 to the area close to the negative ϵ_2 axis, while the analysis for the Takens–Bogdanov case would apply to the larger shaded region.

We identify several physical situations where a Takens–Bogdanov point occurs, and evaluate the coefficients of the amplitude equations for each of them. We then look for stable patterns by integrating the amplitude equations in time. In most cases, we find steady solutions on one side of the Takens–Bogdanov point and time-periodic solutions on the other side with a transition regime in between. The preferred steady patterns are rolls and hexagons, and the preferred periodic patterns are traveling rolls and "wavy rolls (1)", and, in one particular case, oscillating triangles [15]. We note that these were also the patterns predicted in the analysis of the Hopf bifurcation [5]. We do not find a transition directly from steady to periodic behavior; instead we observe a variety of quasiperiodic and chaotic solutions in the transition regime.

2. Double-layer convection

Fig. 4 illustrates the problem configuration. The upper boundary at $z = l^*$ is kept at a constant temperature θ_0^*, and the lower boundary at $z = 0$ is kept at a higher constant temperature $\theta_1^* = \theta_0^* + \Delta\theta^*$. At the temperature of the top plate, fluid i has coefficient of cubical expansion $\hat{\alpha}_i$, thermal diffusivity κ_i, thermal conductivity k_i, viscosity μ_i, density ρ_i, and kinematic viscosity $\nu_i = \mu_i/\rho_i$. S^* is the dimensional interfacial tension coefficient. The average height of the lower fluid (fluid 1) is l_1^*. The average height of the upper fluid (fluid 2) is $l^* - l_1^* = l_2^*$. Length is made dimensionless with the plate separation l^*, time with l^{*2}/κ_1, velocity with κ_1/l^*, and pressure with $(\rho_1\kappa_1^2)/l^{*2}$. The dimensionless interface position is denoted by $z = l_1 + h(x, y, t)$, velocity by $\boldsymbol{v} = (u, v, w)$, the pressure by p and the temperature by θ. The dimensionless temperature is denoted by $\theta = (\theta^* - \theta_0^*)/\Delta\theta^*$ (asterisks denote dimensional quantities).

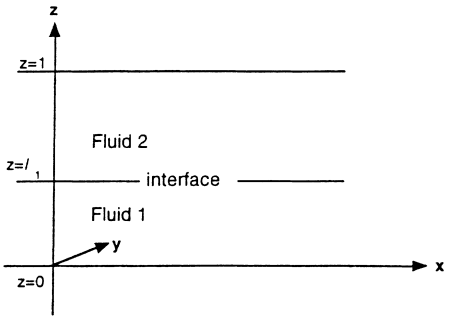

Fig. 4. Problem definition.

There are six independent dimensionless ratios arising from the stratification in the fluid properties: $m = \mu_1/\mu_2$, $r = \rho_1/\rho_2$, $\gamma = \kappa_1/\kappa_2$, $\zeta = k_1/k_2$, $\beta = \hat{\alpha}_1/\hat{\alpha}_2$, $l_1 = l_1^*/l^* = 1 - l_2$, where $l_2 = l_2^*/l^*$. There are four more independent parameters: a Rayleigh number $R = g\hat{\alpha}_1\Delta\theta^* l^{*3}/(\kappa_1\nu_1)$, a Prandtl number $P = \nu_1/\kappa_1$, a dimensionless measure of the temperature difference between the plates $\hat{\alpha}_1\Delta\theta^*$ which should be sufficiently small to be consistent with the Oberbeck–Boussinesq approximation, and a surface tension parameter $S = S^* l^*/(\kappa_1\mu_1)$. Here, $\hat{\alpha}_1\Delta\theta^* = RP/G$, where $G = g(l^*)^3/\kappa_1^2$. The gravity parameter G appears in the base pressure field, and enters the analysis through the interfacial normal stress condition if there is a density jump across the interface.

In each fluid, the governing equations are the heat transport equation, the Navier–Stokes equation and incompressibility. The boundary conditions are zero velocity and constant temperature: $\theta = 1$ at $z = 0$, $\theta = 0$ at $z = 1$. The interface is at $z = l_1 + h(x, y, t)$. The conditions to be satisfied at the interface are continuity of velocity, temperature and heat flux, and balance of tractions.

2.1. Base Solution

A base solution to the problem is given by

$$h = 0, \quad \boldsymbol{v} = \boldsymbol{0}, \quad \theta = \begin{cases} 1 - A_1 z & \text{for} \quad 0 \le z \le l_1, \\ A_2(1 - z) & \text{for} \quad l_1 \le z \le 1, \end{cases} \tag{1}$$

$A_1 = 1/(l_1 + \zeta l_2)$, $A_2 = \zeta A_1$. Note the corresponding pressure field is found in Joseph and Renardy [16] and enters into the interface continuity conditions in the perturbation equations.

2.2. Perturbation equations

We denote by $\tilde{\theta}$ the difference between θ and the base solution (1), and by $\tilde{p}$ the difference between p and the base solution. The perturbation stress tensor is denoted $\tilde{\boldsymbol{T}} = P[\nabla\boldsymbol{v} + (\nabla\boldsymbol{v})^{\mathrm{T}}] - \tilde{p}\boldsymbol{1}$ in fluid 1, and $(P/m)[\nabla\boldsymbol{v} + (\nabla\boldsymbol{v})^{\mathrm{T}}] - \tilde{p}\boldsymbol{1}$ in fluid 2, where $(\nabla\boldsymbol{v})^{\mathrm{T}}$ denotes the transpose of $\nabla\boldsymbol{v}$. The governing equations are, for $0 \le z \le l_1 + h(x, y, t)$ (layer 1), the heat transport equation $\dot{\tilde{\theta}} - A_1 w - \Delta\tilde{\theta} = -(\boldsymbol{v}\cdot\nabla)\tilde{\theta}$, the momentum equation $\dot{\boldsymbol{v}} - P\Delta\boldsymbol{v} + \nabla\tilde{p} - RP\tilde{\theta}\boldsymbol{e}_z = -(\boldsymbol{v}\cdot\nabla)\boldsymbol{v}$, and for $l_1 + h(x, y, t) \le z \le 1$ (layer 2), $\dot{\tilde{\theta}} - A_2 w - \Delta\tilde{\theta}/\gamma = -(\boldsymbol{v}\cdot\nabla)\tilde{\theta}$, $\dot{\boldsymbol{v}} - (r/m)P\Delta\boldsymbol{v} + r\nabla\tilde{p} - (RP/\beta)\tilde{\theta}\boldsymbol{e}_z = -(\boldsymbol{v}\cdot\nabla)\boldsymbol{v}$, together with incompressibility $\operatorname{div}\boldsymbol{v} = 0$. The boundary conditions at the walls $z = 0$ and $z = 1$ are $\boldsymbol{v} = \boldsymbol{0}$, $\tilde{\theta} = 0$. Let $\boldsymbol{t}_1, \boldsymbol{t}_2$ denote two unit tangent vectors and let $\boldsymbol{n}$ be a unit normal to the interface. By $[\![\cdot]\!]$ we denote the jump of a quantity across the interface, i.e. its value in fluid 1 minus its value in fluid 2. The interface conditions at $z = l_1 + h$ are the continuity of velocity, shear stress, the jump in the normal stress is balanced by surface tension and curvature, continuity of temperature, continuity of heat flux, and the kinematic condition. These

are, respectively,

$$[\![\boldsymbol{v}]\!] = \boldsymbol{0}, \qquad [\![\boldsymbol{t}_i \cdot \tilde{\boldsymbol{T}} \cdot \boldsymbol{n}]\!] = 0, \quad i = 1, 2, \tag{2}$$

$$[\![\boldsymbol{n} \cdot \tilde{\boldsymbol{T}} \cdot \boldsymbol{n}]\!] = -M_1 h + M_2 h^2 + \frac{PS\left\{\frac{\partial^2 h}{\partial x^2}\left[1 + \left(\frac{\partial h}{\partial y}\right)^2\right] + \frac{\partial^2 h}{\partial y^2}\left[1 + \left(\frac{\partial h}{\partial x}\right)^2\right] - 2\frac{\partial^2 h}{\partial x \partial y}\frac{\partial h}{\partial x}\frac{\partial h}{\partial y}\right\}}{[1 + (\nabla h)^2]^{3/2}},$$

$$[\![\tilde{\theta}]\!] = h(A_1 - A_2), \qquad [\![k\boldsymbol{n} \cdot \nabla\tilde{\theta}]\!] = 0, \qquad \dot{h} + u\frac{\partial h}{\partial x} + v\frac{\partial h}{\partial y} = w,$$

$$M_1 = G\left(1 - \frac{1}{r}\right) + RPA_2 l_2\left(\frac{1}{r\beta} - 1\right), \qquad M_2 = \frac{RP}{2}\left(\frac{A_2}{r\beta} - A_1\right).$$

Terms up to third order are required in the derivation of the amplitude equations. The momentum and heat transport equations contribute quadratic nonlinearities. The interface conditions (2), expanded in Taylor series about the known position $z = l_1$ and truncated, yield quadratic and cubic nonlinearities. These are lengthy expressions and can be found in ([16] Chapter III) and [2]. We denote by Φ the solution vector $(u, v, w, \tilde{p}, \tilde{\theta}, h)$ and write the system of equations, boundary and interface conditions in the schematic form

$$L(\Phi) = N_2(\Phi, \Phi) + N_3(\Phi, \Phi, \Phi), \tag{3}$$

where L, N_2, N_3 represent the linear, quadratic and cubic operators, respectively. We perform a three-dimensional bifurcation analysis.

3. Examples of Takens–Bogdanov points

The examples investigated in this section are taken from [4,5]. The work in [5] was motivated by experiments on Fluorinert lying under silicone oil Rhodorsil 47v10. A fictitious fluid, Anderinert, was inadvertently created by a software package which was used by the experimental group to convert units. Anderinert has a thermal diffusivity 3.24 times that of Fluorinert. As it turns out, the onset of instability in the Fluorinert/silicone oil system is always to a steady mode, while the Anderinert system has a window of parameters where a Hopf onset occurs. The coalescence of two real eigenvalues to form a complex conjugate pair as shown in Fig. 2 occurs in both systems, but for the Fluorinert system it only happens after the system has already become unstable, and oscillatory onset does not happen unless the spatial period of solutions is artificially constrained. Indeed, the experiments of [8] show a steady bifurcation occurring first, and then periodic solutions arise from a secondary bifurcation. In both the Fluorinert/silicone oil and Anderinert/silicone oil systems, the onset of instability is close to a Takens–Bogdanov point if l_1 is chosen appropriately. Below, we shall pursue the parameters for both of these systems, as well as those used in [4].

The fluid parameters for the Anderinert/silicone oil system are given in row (a) of Table 1. Fig. 5 shows the Rayleigh number and wave number at which onset of instability occurs as functions of l_1. Oscillatory onset occurs in the interval $0.486 \leq l_1 \leq 0.504$. The endpoints of this interval are not Takens–Bogdanov points, because the onset of instability shifts to a different wave number: at $l_1 = 0.486$, there is an interaction of a real mode with wavenumber 6 and Hopf mode with wavenumber 5.3. At $l_1 = 0.504$, there is an interaction of a real mode with wavenumber 5.6 and a Hopf mode with wavenumber 5.2. We find Takens–Bogdanov points if we fix the wavenumber, say at 5.3, and this is illustrated in Fig. 6. The detailed numerical values for the left and right hand ends of the band of Hopf modes in Fig. 6 are given in Table 2. We note that throughout the interval where Hopf modes exist, the frequencies of the oscillatory modes remain small. In dimensionless terms, the largest frequencies we found are around 5 (for

Table 1
(a) The first row gives the fluid parameters for Anderinert/silicone oil. For interfacial tension, a value of 20 in CGS units is used. (b) The second row gives the parameters for Fluorinert/silicone oil. (c) The third row gives parameters for our. description of the example used in Fig. 2 of [17]. In their notation, $(\alpha, \kappa, \rho, \lambda, a)$ correspond to our $(\beta, \gamma, r, \zeta, l_2/l_1)$. Rl_1^4 is their Rayleigh number, their wavenumber k_0 is αl_1

	P	G	S	γ	β	r	ζ	m
(a)	125.3	1.571×10^9	8.3×10^4	1.299	0.926	2.092	0.5385	2.929
(b)	406.3	1.65×10^{10}	2.7×10^5	0.401	0.926	2.092	0.5385	2.929
(c)	10^5	10^{10}	10^3	2	0.2	10	1	1

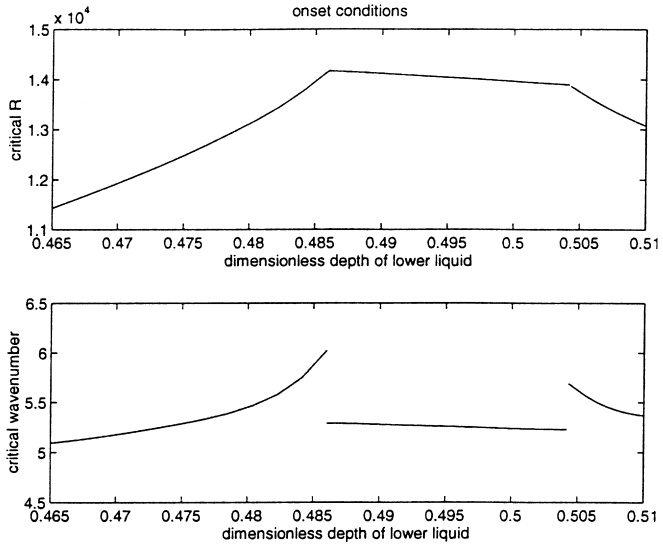

Fig. 5. Onset conditions for the Anderinert/silicone oil system with fluid parameters as in row (a) of Table 1.

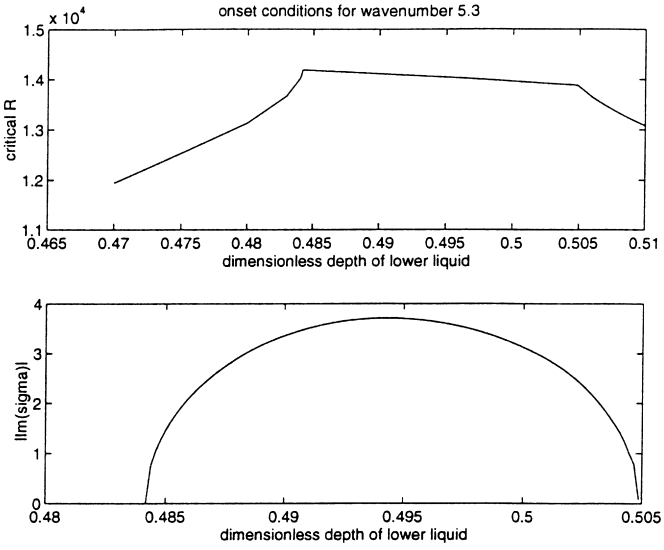

Fig. 6. Onset conditions for row (a) of Table 1 when the wavenumber is fixed at $\alpha = 5.3$.

Table 2
The values of the lower fluid depth l_1, Rayleigh numbers R and the least stable eigenvalues σ for the Anderinert/silicone oil system are given for points close to the left and right hand ends of the Hopf onset range of Fig. 6, wavenumber 5.3, showing the sensitivity with respect to the parameters. In the cases below, as R increases, complex conjugate eigenvalues turn into reals

l_1	R	σ
0.48417472	14190.4625	-0.0001 ± 0.0006i
0.48417472	14190.4629	0.00008
0.48417472	14190.4629	-0.0003
0.50487	13883.1828	-0.0035 ± 0.0037i
0.50487	13883.1853	0.00002&-0.00692

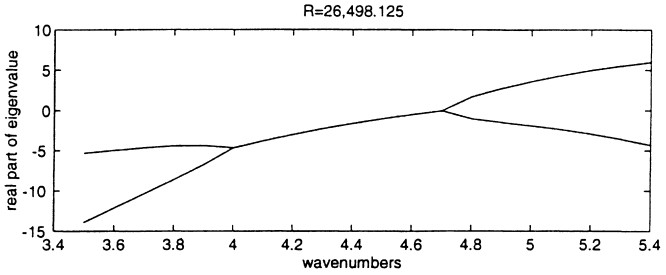

Fig. 7. Fluorinert and silicone oil system with $l_1 = 0.423$, $R = 26\,498.125$. The Takens–Bogdanov point is close to $\alpha = 4.711$.

Table 3
Values of the wavenumber, Rayleigh number and least stable eigenvalues are given for the Fluorinert system, second row of Table 1, with $l_1 = 0.423$ fixed

α	R	σ
4.711	26498.125	-0.006 ± 0.0178i
4.71	26502.5	0.003 ± 0.066i

instance in Fig. 6 the maximum value is between 3 and 4), in contrast α^2 is around 25 (note that the heat equation involves the combination $\dot{\theta} - \Delta\theta$). Hence the assumption of small frequency is actually satisfied throughout the range where Hopf modes exist. The Takens–Bogdanov analysis carried out in this paper applies near either end of this range; a more comprehensive treatment would need to consider the merger of two Takens–Bogdanov points which leads to a more degenerate and complicated bifurcation (see [9,10]).

The fluid parameters for the Fluorinert/silicone oil system are given in the second row of Table 1. If the wave number is unconstrained, the onset of instability is always due to real eigenvalues. However, if we fix the spatial period, there are windows of Hopf onsets and Takens–Bogdanov points in this system as well. This is illustrated in Fig. 7, which shows the eigenvalues as a function of wavenumber for a fixed Rayleigh number and depth ratio numerical values for the Takens–Bogdanov point are given in Table 3.

The third row of Table 1 shows data modeling Fig. 2 of [4]. They give the thermal diffusivity ratio (their κ), $m/(r\beta)$ (their ν/α), m, the conductivity ratio, their wavenumber $k_0 = 2.7$, volume ratio $a = l_2/l_1$. Our wavenumber α is k_0/l_1, their a is our l_2/l_1, their Rayleigh number is Rl_1^4. In their problem, the interface is constrained to remain flat and $P = \infty$. In order to model their problem we choose appropriately large values for our interfacial tension parameter, Prandtl number and G. With our choice of parameters, we examined the second row of their Table 1, where they give $l_1 = 0.5$, their Rayleigh number 1173, frequency $w_0 = 1.29 = \mathrm{Im}\,\sigma l_1^2$. This translates to $R = 18\,768$, $\mathrm{Im}\,\sigma = 5.16$. We find $\mathrm{Im}\,\sigma = 5.26$ and neutral $R = 18\,777$. The variation with respect to wavenumbers was examined at $R = 18\,768$ and the maximum growth rate was attained at $\alpha = 5.2$ rather than 5.4. The small

Table 4
The parameters for the third row of Table 1, with $\alpha = 5.4$ fixed

l_1	R	σ
0.48303	19560.6	0.03±0.006i
0.4837929	19516.5	0.0087±1.54i
0.5199	17850	0.006±0.135i
0.52	17825.390625	−0.04±0.03i
0.52	17825	−0.04±0.08i

difference between our results and theirs may be due to the fact that they use an approximate set of equations for the limit of infinite Prandtl number (Table 4) .

4. Bifurcation analysis at a Hopf bifurcation

We give a brief synopsis leading up to the amplitude equation for solutions in the neighborhood of a Hopf onset, with double periodicity on the hexagonal lattice. These results have appeared in [2,5,16], where the final amplitude equations are given in Birkhoff normal form. In this form, several terms including quadratic terms have been transformed away under suitable coordinate transformations and the amplitude equation is then in its simplest form. The Birkhoff normal form of the amplitude equations is the starting point for the analysis of [15], where a comprehensive analysis of bifurcating periodic solutions with maximal symmetry is given.

Our analysis for the Takens–Bogdanov case will begin with the amplitude equations that result just prior to the transformation to Birkhoff normal form, because it is precisely these coordinate transformations that break down when the frequency tends to zero. In the Takens–Bogdanov case, a straightforward calculation of the generalized eigenfunctions is lengthy so we wish to avoid this; we can find them more efficiently by taking a suitable limit of the Hopf eigenfunctions as the problem approaches the Takens–Bogdanov case. We return to this issue in Section 5.

4.1. Spatial periodicity on the hexagonal lattice

In the x- and y-directions, the solution is assumed to be doubly periodic, e.g., $\tilde{\theta}(\boldsymbol{x} + n_1\boldsymbol{x}_1 + n_2\boldsymbol{x}_2, t) = \tilde{\theta}(\boldsymbol{x}, t)$ for every pair of integers (n_1, n_2), where the vectors $\boldsymbol{x}_1$ and $\boldsymbol{x}_2$ span a hexagonal lattice of period W : $\boldsymbol{x}_1 = W \cdot (\sqrt{3}/2, 1/2, 0), \boldsymbol{x}_2 = W \cdot (0, 1, 0)$. The lattice obtained from this double periodicity is invariant under the symmetries of the hexagon; that is, rotation by multiples of 60°, reflection across the vectors $\boldsymbol{a}_i$ defined by $\boldsymbol{a}_1 = (4\pi/W\sqrt{3})(1, 0, 0), \boldsymbol{a}_2 = (4\pi/W\sqrt{3})(-1/2, \sqrt{3}/2, 0), \boldsymbol{a}_3 = -\boldsymbol{a}_1 - \boldsymbol{a}_2$, and reflection across axes perpendicular to the $\boldsymbol{a}_i$. The same periodicity condition holds for $\tilde{\theta}, \boldsymbol{v}, \tilde{h}$ and $\tilde{p}$. These variables are expanded in Fourier series; e.g., $\tilde{\theta}(x, y, z, t)$ is the sum over k and l of modes $\tilde{\theta}_{kl}(z, t)\mathrm{e}^{\mathrm{i}k\boldsymbol{a}_1\cdot\boldsymbol{x}+\mathrm{i}l\boldsymbol{a}_2\cdot\boldsymbol{x}}$. We next recall the results for a Hopf bifurcation, show the amplitude equation for this case, and then later build the connection to the Takens–Bogdanov case.

For the linearized problem (Section 3), the method of separation of variables yields $\tilde{\theta}_{kl} = \mathrm{e}^{\sigma t}\tilde{\theta}(z)$, and similarly for $\boldsymbol{v}, \tilde{p}, \tilde{h}$. This leads to an eigenvalue problem for σ, in which the results do not depend on the direction of the vector $k\boldsymbol{a}_1 + l\boldsymbol{a}_2$, but on its magnitude α given by $|k\boldsymbol{a}_1 + l\boldsymbol{a}_2| = (4\pi/\sqrt{3}W)(k^2 + l^2 - kl)^{1/2}$; the wavenumber α denotes the critical value determined in Section 3. This equation determines the period W of the lattice. The factor $k^2 + l^2 - kl$ can be 0, 1, 3, 4, 7, ... The mean flow mode $k = l = 0$ is not of interest in the linear problem, but will enter into the nonlinear interactions. The smallest nonzero value of $k^2 + l^2 - kl$ is 1, for which W is $(4\pi/\sqrt{3}\alpha)$. This occurs for six possible pairs $(k, l) : (\pm1, 0), (0, \pm1), (1, 1)$, and $(-1, -1)$, yielding a sixfold degeneracy of the corresponding eigenvalue. We pursue this case where the lattice size fits exactly into the critical period, and look

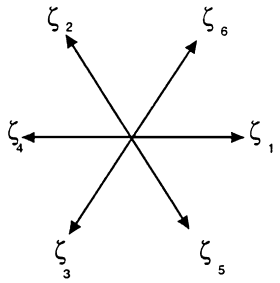

Fig. 8. The eigenvectors ζ_i denote waves traveling to the six vertices of a hexagon constructed with vectors $\boldsymbol{a}_1, \boldsymbol{a}_2, \boldsymbol{a}_3, -\boldsymbol{a}_1, -\boldsymbol{a}_2, -\boldsymbol{a}_3$. The corresponding wave amplitudes are z_i.

at the nonlinear interaction generated by the six Fourier modes. (If $k^2 + l^2 - kl$ is chosen larger than one, then we would seek solutions on a larger lattice with period a multiple of the critical one.) At criticality, there is a complex conjugate pair of eigenvalues $\sigma = \pm \mathrm{i}\omega$ which has six eigenfunctions denoted by ζ_k, corresponding to the six values of (k, l). The eigenfunctions computed in Section 3 correspond to the case of $l = 0,\ k = 1$ and are denoted by ζ_1 and of the form $\tilde{\zeta}(z)\exp(\mathrm{i}\boldsymbol{a}_1 \cdot \boldsymbol{x})$, where $\boldsymbol{a}_1 = (\alpha_c, 0, 0)$. The vectors $\pm\boldsymbol{a}_1,\ \pm\boldsymbol{a}_2$ and $\pm\boldsymbol{a}_3$ emanate from the center of a hexagon and terminate at its six vertices. The critical eigenfunctions are waves propagating in the directions of the vertices. Fig. 8 illustrates the eigenvectors.

Let the parameter λ denote a set of bifurcation parameters, e.g., the difference between the Rayleigh number and its critical value $R - R_C$, or one of the fluid property ratios. Close to criticality, an initial disturbance proportional to $\zeta_k(\lambda)$ evolves as $\exp[-\mu(\lambda)t]$. At criticality, $\lambda = 0,\ \mu(0) = \mathrm{i}\omega$.

We denote the complex time-dependent amplitude function of the wave propagating in the direction of $\boldsymbol{a}_i$ by z_i. In order to obtain an amplitude evolution equation for the weakly nonlinear analysis, the governing equations are reduced to a system of ordinary differential equations in the 12-dimensional space $\mathbb{R}^{12}$ by invoking the center manifold theorem which says roughly that in the neighborhood of criticality, the dynamics is governed by interactions among the six critical modes. This allows us to write the solution in the form

$$\Phi = \Phi_1 + \Psi_2 + \text{higher order terms}, \tag{4}$$

$$\Phi_1 = \sum_{i=1}^{6} z_i \zeta_i + \sum_{i=1}^{6} \bar{z}_i \bar{\zeta}_i, \qquad \Psi_2 = 2\,\mathrm{Re}\left(\sum_{i,j=1}^{6} z_i z_j \psi_{ij} + z_i \bar{z}_j \chi_{ij} \right),$$

where the interaction terms ψ_{ij}, χ_{ij} are found by certain projections in the center manifold reduction scheme. Details of the derivation are contained in [2,16]. The following amplitude equation is obtained at the bifurcation point:

$$\frac{\mathrm{d}z_i}{\mathrm{d}t} + F_i(z_1, z_2, z_3, z_4, z_5, z_6, \lambda) = 0, \quad i = 1, \ldots, 6, \tag{5}$$

where $F_i, i = 2, \ldots, 6$ can be retrieved from F_1 by permutation of the arguments:

$$\begin{aligned}
F_2(z_1, z_2, z_3, z_4, z_5, z_6) &= F_1(z_2, z_3, z_1, z_5, z_6, z_4),\\
F_3(z_1, z_2, z_3, z_4, z_5, z_6) &= F_1(z_3, z_1, z_2, z_6, z_4, z_5),\\
F_4(z_1, z_2, z_3, z_4, z_5, z_6) &= F_1(z_4, z_5, z_6, z_1, z_2, z_3),\\
F_5(z_1, z_2, z_3, z_4, z_5, z_6) &= F_1(z_5, z_6, z_4, z_2, z_3, z_1),\\
F_6(z_1, z_2, z_3, z_4, z_5, z_6) &= F_1(z_6, z_4, z_5, z_3, z_1, z_2),
\end{aligned} \tag{6}$$

and

$$
\begin{aligned}
F_1(z_1, z_2, z_3, z_4, z_5, z_6, \lambda) &= \mu(\lambda)z_1 + \beta_1(\lambda)z_5z_6 + \beta_2(\lambda)\bar{z}_2\bar{z}_3 + \beta_3(\lambda)(z_5\bar{z}_3 + z_6\bar{z}_2) + \gamma_1(\lambda)|z_1|^2z_1 \\
&+\gamma_2(\lambda)|z_4|^2z_1 + \gamma_3(\lambda)z_1^2z_4 + \gamma_4(\lambda)\bar{z}_4^2\bar{z}_1 + \gamma_5(\lambda)|z_1|^2\bar{z}_4 + \gamma_6(\lambda)|z_4|^2\bar{z}_4 \\
&+\gamma_7(\lambda)(|z_2|^2 + |z_3|^2)z_1 + \gamma_8(\lambda)(|z_2|^2 + |z_3|^2)\bar{z}_4 + \gamma_9(\lambda)(|z_5|^2 + |z_6|^2)z_1 \\
&+\gamma_{10}(\lambda)(|z_5|^2 + |z_6|^2)\bar{z}_4 + \gamma_{11}(\lambda)(z_2z_5 + z_3z_6)z_1 + \gamma_{12}(\lambda)(z_2z_5 + z_3z_6)\bar{z}_4 \\
&+\gamma_{13}(\lambda)(\bar{z}_2\bar{z}_5 + \bar{z}_3\bar{z}_6)z_1 + \gamma_{14}(\lambda)(\bar{z}_2\bar{z}_5 + \bar{z}_3\bar{z}_6)\bar{z}_4. \qquad (7)
\end{aligned}
$$

Terms of higher than third degree have been ignored. We remark that, in order to remove certain degeneracies, it is necessary to include some fifth-order terms in the analysis of the Hopf bifurcation [15]. This is not the case for the Takens–Bogdanov analysis, because the degeneracy is also removed by quadratic terms. These quadratic terms transform away in the Birkhoff normal form for the Hopf bifurcation, but this transformation breaks down in the Takens–Bogdanov limit. The coefficients β_i and γ_i are the Landau constants defined in [2] and in ([16], Chapter III.7).

The numerical code for calculating the Landau coefficients is developed from that used in [2,5]. We comment in passing that, in the process, an error has been detected in the calculation of χ_{15} and χ_{24}. This affects the value of the Landau coefficient α_4 in [2,5]. It turns out that the qualitative nature of results in [2] is unaffected. The problem studied in [2] is the two-layer Bénard problem in the case where oscillatory onset arises due to the coupling between the Bénard instability and the interface motion; it is found in this case that the 11 solutions found in [15] are unstable for the three data considered in [2].

In the present problem, where oscillatory onset arises due to the coupling of the motions in both layers, with negligible interface motion, the results are different, and stable periodic branches are found to exist. The revised results for [5] are contained in [18]. The results indicate that the periodic solutions most likely to be stable are the traveling rolls and the wavy rolls (1).

5. Bifurcation analysis at a Takens–Bogdanov point

In the linearized stability analysis, we focus on an onset condition with a double zero eigenvalue. Associated with this, there are six eigenfunctions denoted by ζ_k, and six generalized eigenfunctions denoted by ξ_k. We consider this as a limiting case of the Hopf bifurcation analysis. As an example of the limits, we consider the case of the 2×2 matrices

$$
D_1 = \begin{pmatrix} 0 & 1 \\ 0 & 0 \end{pmatrix}, \qquad D_2 = \begin{pmatrix} 0 & 1 \\ -\epsilon & 0 \end{pmatrix}.
$$

The second matrix is a perturbation of the first; D_1 has a double zero eigenvalue, and D_2 (the Hopf case) has complex eigenvalues $\mu = \mathrm{i}\sqrt{\epsilon}$ and $\bar{\mu} = -\mathrm{i}\sqrt{\epsilon}$. The eigenvectors for the Hopf case are

$$
\begin{pmatrix} 1 \\ \mathrm{i}\sqrt{\epsilon} \end{pmatrix} \text{and} \begin{pmatrix} 1 \\ -\mathrm{i}\sqrt{\epsilon} \end{pmatrix}.
$$

In analogy with the present problem, we refer to these as ζ_1 and $\bar{\zeta}_4$, respectively. As $\epsilon \to 0$, ζ_1 and $\bar{\zeta}_4$ become the same and the set of eigenvectors is no longer linearly independent. D_1 has eigenvector $\binom{1}{0}$. The generalized eigenvector ξ satisfies $D_1\xi =$ the eigenvector, so $\xi = \binom{0}{1}$. The eigenvector is $(\zeta_1 + \bar{\zeta}_4)/2$ and the generalized eigenvector is $(\zeta_1 - \bar{\zeta}_4)/(\mu - \bar{\mu})$. Note that as $\epsilon \to 0$, the latter approaches a finite limit due to the expression

$\mu-\bar{\mu}$ in the denominator. Thus, $(\zeta_1+\bar{\zeta}_4)/2$ and $(\zeta_1-\bar{\zeta}_4)/(\mu-\bar{\mu})$ provide a linearly independent basis for the eigenspace in the limit as $\epsilon\to 0$.

We return to the Hopf bifurcation on the hexagonal lattice, and consider the component of the solution Φ_1 proportional to $\exp(\mathrm{i}\alpha x)$. We express this in terms of the eigenvector and generalized eigenvector of the Takens–Bogdanov problem:

$$z_1\zeta_1+\bar{z}_4\bar{\zeta}_4=v_1\frac{\zeta_1+\bar{\zeta}_4}{2}-w_1\frac{\zeta_1-\bar{\zeta}_4}{\mu-\bar{\mu}}. \tag{8}$$

The amplitude functions for the Takens–Bogdanov case are v_1 and w_1. From this, we see that $z_1=v_1/2-w_1/(\mu-\bar{\mu}), \bar{z}_4=v_1/2+w_1/(\mu-\bar{\mu}), z_2=v_2/2-w_2/(\mu-\bar{\mu}), \bar{z}_5=v_2/2+w_2/(\mu-\bar{\mu}), z_3=v_3/2-w_3/(\mu-\bar{\mu})$, and $\bar{z}_6=v_3/2+w_3/(\mu-\bar{\mu})$. The amplitude equations (7) have the form $\dot{z}_1+\mu z_1=$ nonlinear terms, and $\dot{\bar{z}}_4+\bar{\mu}\bar{z}_4=$ nonlinear terms (this is obtained from (7) with $z_1\to z_4$, $z_2\to z_5$, $z_3\to z_6$). Our aim is to obtain amplitude equations for the v_1 and w_1. Therefore, we add the $\dot{z}_1$-and $\dot{\bar{z}}_4$-equations, and use $z_1+\bar{z}_4=v_1$ and $\mu z_1+\bar{\mu}\bar{z}_4=[(\mu+\bar{\mu})/2]v_1-w_1$, to obtain $\dot{v}_1+[(\mu+\bar{\mu})/2]v_1-w_1=$ nonlinear terms. We subtract the equations, multiply through by $(\mu-\bar{\mu})/2$, and obtain $\dot{w}_1-((\mu-\bar{\mu})^2/4)v_1+([\mu+\bar{\mu}]/2)w_1=$ nonlinear terms. We define bifurcation parameters $\epsilon_1=(\mu+\bar{\mu})/2$ and $\epsilon_2=(\mu-\bar{\mu})^2/4$. Our previously defined notation λ represents the set (ϵ_1,ϵ_2). On the Hopf side of the Takens–Bogdanov point, $\mu(0)=\mathrm{i}\omega$ so $\epsilon_1=0$, $\epsilon_2=-\omega^2$ ($\omega\to 0$). The base solution is unstable for $\epsilon_1<0$ (since $\zeta_k\sim\exp(-\mu(\lambda)t)$). This leads to amplitude equations as follows (up to cubic order)

$$\begin{aligned}0=&\dot{w}_1+\epsilon_1w_1-\epsilon_2v_1+b_1\bar{w}_2\bar{w}_3+b_2\bar{v}_2\bar{v}_3+b_3(\bar{w}_2\bar{v}_3+\bar{w}_3\bar{v}_2)+c_1|w_1|^2w_1+c_2|w_1|^2v_1\\&+c_3|v_1|^2w_1+c_4|v_1|^2v_1+c_5v_1^2\bar{w}_1+c_6w_1^2\bar{v}_1+c_7(|v_2|^2+|v_3|^2)v_1+c_8(|v_2|^2+|v_3|^2)w_1\\&+c_9(v_2\bar{w}_2+v_3\bar{w}_3)v_1+c_{10}(\bar{v}_2w_2+\bar{v}_3w_3)v_1+\dots,\end{aligned} \tag{9}$$

$$\begin{aligned}0=&\dot{v}_1-w_1+\epsilon_1v_1+\tilde{b}_1\bar{w}_2\bar{w}_3+\tilde{b}_2\bar{v}_2\bar{v}_3+\tilde{b}_3(\bar{w}_2\bar{v}_3+\bar{w}_3\bar{v}_2)+\tilde{c}_1|w_1|^2w_1+\tilde{c}_2|w_1|^2v_1\\&+\tilde{c}_3|v_1|^2w_1+\tilde{c}_4|v_1|^2v_1+\tilde{c}_5v_1^2\bar{w}_1+\tilde{c}_6w_1^2\bar{v}_1+\tilde{c}_7(|v_2|^2+|v_3|^2)v_1+\tilde{c}_8(|v_2|^2+|v_3|^2)w_1\\&+\tilde{c}_9(v_2\bar{w}_2+v_3\bar{w}_3)v_1+\tilde{c}_{10}(\bar{v}_2w_2+\bar{v}_3w_3)v_1+\dots,\end{aligned} \tag{10}$$

where the coefficients $b_i, c_i, \tilde{b}_i, \tilde{c}_i$ are real. The remaining equations are found by cyclic permutation of the indices. We can transform away the ϵ_1-term in Eq. (10) by the substitution $\hat{w}_1=w_1-\epsilon_1v_1$. This yields the new equations

$$\begin{aligned}0=&\dot{w}_1+2\epsilon_1w_1-\epsilon_2v_1+b_1\bar{w}_2\bar{w}_3+b_2\bar{v}_2\bar{v}_3+b_3(\bar{w}_2\bar{v}_3+\bar{w}_3\bar{v}_2)+c_1|w_1|^2w_1+c_2|w_1|^2v_1\\&+c_3|v_1|^2w_1+c_4|v_1|^2v_1+c_5v_1^2\bar{w}_1+c_6w_1^2\bar{v}_1+c_7(|v_2|^2+|v_3|^2)v_1+c_8(|v_2|^2+|v_3|^2)w_1\\&+c_9(v_2\bar{w}_2+v_3\bar{w}_3)v_1+c_{10}(\bar{v}_2w_2+\bar{v}_3w_3)v_1+\dots,\end{aligned} \tag{11}$$

$$\begin{aligned}0=&\dot{v}_1-w_1+\tilde{b}_1\bar{w}_2\bar{w}_3+\tilde{b}_2\bar{v}_2\bar{v}_3+\tilde{b}_3(\bar{w}_2\bar{v}_3+\bar{w}_3\bar{v}_2)+\tilde{c}_1|w_1|^2w_1+\tilde{c}_2|w_1|^2v_1+\tilde{c}_3|v_1|^2w_1\\&+\tilde{c}_4|v_1|^2v_1+\tilde{c}_5v_1^2\bar{w}_1+\tilde{c}_6w_1^2\bar{v}_1+\tilde{c}_7(|v_2|^2+|v_3|^2)v_1+\tilde{c}_8(|v_2|^2+|v_3|^2)w_1\\&+\tilde{c}_9(v_2\bar{w}_2+v_3\bar{w}_3)v_1+\tilde{c}_{10}(\bar{v}_2w_2+\bar{v}_3w_3)v_1+\dots\end{aligned} \tag{12}$$

Here we have suppressed the hats, as well as terms which represent $\mathrm{O}(\epsilon)$ perturbations to the coefficients. The following analysis will proceed on the basis of Eqs. (11) and (12).

The small parameters ϵ_1 and ϵ_2 determine the behavior of the linearized system. We note that the eigenvalues of the linearization are

$$-\epsilon_1\pm\sqrt{\epsilon_1^2+\epsilon_2}. \tag{13}$$

Thus, we have real eigenvalues if $\epsilon_2 > -\epsilon_1^2$ and complex eigenvalues if $\epsilon_2 < -\epsilon_1^2$. Moreover, $-\epsilon_1$ is the average of the two eigenvalues, and in the case of complex eigenvalues, the onset of instability (Hopf bifurcation) occurs when $\epsilon_1 = 0$.

5.1. Rescaling of the equations

The aim of introducing new scales is to balance the linear terms with some of the nonlinear terms, while keeping the symmetries in the problem as they are. Thus, the v_i are scaled in the same manner, and the w_i also. According to Eq. (12), we ought to scale $\dot{v}_i$ in the same manner as w_i, and Eq. (11) suggests scaling $\dot{w}_i$ in the same way as $\epsilon_2 v_i$. We can balance linear and quadratic terms in Eq. (11) if we scale $\dot{w}_i$ in the same fashion as v_i^2. For the case where the coefficients of the quadratic terms are small, and also to study the pattern of rolls for which quadratic interaction terms vanish identically, it is of interest to consider a second scaling where $\dot{w}_i$ is scaled in the same way as v_i^3. These considerations lead to the following two cases.

5.1.1. Case A

Here the coefficients of quadratic terms are assumed to be of order one, and cubic terms enter only as a lower order perturbation. $\mathrm{d}/\mathrm{d}t = \sqrt{\epsilon}\mathrm{d}/\mathrm{d}\tau$, $v_i = \epsilon\tilde{v}_i$, $\epsilon_2 = \pm\epsilon$, $w_i = \epsilon^{3/2}\tilde{w}_i$, $\epsilon_1 = \gamma\epsilon$. To simplify notation, we have written v_i, w_i for $\tilde{v}_i$, $\tilde{w}_i$ in the equations that follow, and we now use a dot to denote $\mathrm{d}/\mathrm{d}\tau$. This leads to $\dot{v}_1 - w_1 + \sqrt{\epsilon}\tilde{b}_2\bar{v}_2\bar{v}_3 = 0$ and $\dot{w}_1 \mp v_1 + b_2\bar{v}_2\bar{v}_3 + \sqrt{\epsilon}(2\gamma w_1 + b_3(\bar{w}_2\bar{v}_3 + \bar{w}_3\bar{v}_2)) = 0$. These combine into one equation:

$$\ddot{v}_1 \mp v_1 + b_2\bar{v}_2\bar{v}_3 + \sqrt{\epsilon}[2\gamma\dot{v}_1 + (\dot{\bar{v}}_2\bar{v}_3 + \dot{\bar{v}}_3\bar{v}_2)(\tilde{b}_2 + b_3)] = 0.$$

5.1.2. Case B

The coefficients of the quadratic terms are small (this scaling is also appropriate for rolls for which the quadratic terms vanish): $\mathrm{d}/\mathrm{d}t = \epsilon\mathrm{d}/\mathrm{d}\tau$, $v_i = \epsilon\tilde{v}_i$, $w_i = \epsilon^2\tilde{w}_i$, $b_i = \epsilon\hat{b}_i$, $\tilde{b}_i = \epsilon\hat{\tilde{b}}_i$, $\epsilon_2 = \pm\epsilon^2$, $\epsilon_1 = \gamma\epsilon^2$.

$$\begin{aligned}
&\dot{v}_1 - w_1 + \epsilon(\hat{\tilde{b}}_2\bar{v}_2\bar{v}_3 + \tilde{c}_4|v_1|^2v_1 + \tilde{c}_7(|v_2| + |v_3|^2)v_1) = 0,\\
&\dot{w}_1 \mp v_1 + \hat{b}_2\bar{v}_2\bar{v}_3 + c_4|v_1|^2v_1 + c_7(|v_2|^2 + |v_3|^2)v_1 + \epsilon[2\gamma w_1 + \hat{b}_3(\bar{w}_2\bar{v}_3 + \bar{w}_3\bar{v}_2)\\
&\quad + c_3|v_1|^2w_1 + c_5v_1^2\bar{w}_1 + c_8(|v_2|^2 + |v_3|^2)w_1 + c_9(\bar{w}_2v_2 + \bar{w}_3v_3)v_1\\
&\quad + c_{10}(w_2\bar{v}_2 + w_3\bar{v}_3)v_1)] = 0.
\end{aligned} \tag{14}$$

Elimination yields:

$$\begin{aligned}
&\ddot{v}_1 \mp v_1 + \hat{b}_2\bar{v}_2\bar{v}_3 + c_4|v_1|^2v_1 + c_7(|v_2|^2 + |v_3|^2)v_1 + \epsilon[2\gamma\dot{v}_1 + (\hat{b}_3 + \hat{\tilde{b}}_2)(\dot{\bar{v}}_2\bar{v}_3 + \dot{\bar{v}}_3\bar{v}_2)\\
&\quad + (c_3 + 2\tilde{c}_4)|v_1|^2\dot{v}_1 + (c_5 + \tilde{c}_4)v_1^2\dot{\bar{v}}_1 + (c_8 + \tilde{c}_7)(|v_2|^2 + |v_3|^2)\dot{v}_1 + (c_9 + \tilde{c}_7)(\dot{\bar{v}}_2v_2 + \dot{\bar{v}}_3v_3)v_1\\
&\quad + (c_{10} + \tilde{c}_7)(\dot{v}_2\bar{v}_2 + \dot{v}_3\bar{v}_3)v_1] = 0.
\end{aligned} \tag{15}$$

In the following, we discuss various types of solutions for these equations. We shall focus on Case B, since first, the equations for Case A are a subset of those for Case B, and second, the equations for Case A are too severely truncated to capture important aspects of the dynamics; for instance, they do not allow for rolls solutions or for stable steady hexagons. In the following discussion, we shall drop the hat on the b_i and $\tilde{b}_i$ in Eq. (15).

We note that for $\epsilon = 0$, the Eq. (15) is a Hamiltonian system with Hamiltonian

$$H = \frac{1}{2}\sum_{i=1}^{3}|\dot{v}_i|^2 \mp \frac{1}{2}\sum_{i=1}^{3}|v_i|^2 + b_2\,\mathrm{Re}(\bar{v}_1\bar{v}_2\bar{v}_3) + \frac{1}{4}c_4\sum_{i=1}^{3}|v_i|^4 + \frac{1}{2}c_7(|v_1|^2|v_2|^2 + |v_2|^2|v_3|^2 + |v_3|^2|v_1|^2). \tag{16}$$

(Denote $v_i = x_i + iy_i$, then $H = (1/2)\sum_k p_k^2 + V(q_1, \ldots, q_6)$, where the q_k denote $x_1, y_1, \ldots, x_3, y_3$, $\dot{q}_k = p_k$, the p_k denote $\dot{x}_1, \ldots, \dot{y}_3$, $\dot{p}_k = -\partial V/\partial q_k$.)

It would be possible to subject Eq. (15) to further transformations to achieve a normal form with fewer coefficients involved. We shall not pursue this, since our discussion below focusses on the Hamiltonian system obtained for $\epsilon = 0$, which cannot be simplified further.

5.2. Time-periodic patterns

Our analysis will be concerned mostly with periodic solutions. In contrast to the case of Hopf bifurcation, however, we are not concerned just with the bifurcation of periodic solutions from the rest state. A new possibility in the Takens–Bogdanov case is the secondary bifurcation of periodic solutions from steady states, which we shall investigate in some detail. Other new features include quasiperiodic states and homoclinic or heteroclinic orbits which can arise as limiting cases of periodic orbits.

The patterns found in [15] for the Hopf bifurcation will play an important role in our analysis as well as in the numerical results below. The following is a list of possible steady solutions and of the periodic solutions of [15], together with the symmetries which they satisfy. We note that the translation symmetries of the original problem manifest themselves in Eq. (15) as the symmetry $v_1 \to v_1\exp(2i\alpha)$, $v_2 \to v_2\exp(-i\alpha+i\beta)$, $v_3 \to v_3\exp(-i\alpha-i\beta)$. For the list below, we have placed centers or axes of symmetry conveniently to get the simplest possible form (e.g. hexagons as listed have their center of symmetry at the origin); clearly other solutions (e.g. a two-parameter family of hexagons) can be generated by spatial translations.

The possible steady patterns are as follows:

1. Rolls: $v_2 = v_3 = 0$, v_1 real.
2. Hexagons: $v_1 = v_2 = v_3$ real.
3. Rectangles (patchwork quilt): v_1 real, $v_2 = v_3$ real.

The latter class of solutions is the one referred to as type IV in [19].

The periodic solutions of Roberts, Swift and Wagner [15] are as follows:

1. Standing rolls: $v_2 = v_3 = 0$, v_1 real, $v_1(t + T/2) = -v_1(t)$.
2. Standing hexagons: $v_1 = v_2 = v_3$ real.
3. Standing patchwork quilt: v_1 real, $v_2 = v_3$ real, $v_2(t + T/2) = -v_2(t)$, $v_1(t + T/2) = v_1(t)$.
4. Standing regular triangles: $v_1 = v_2 = v_3$, $v_1(t + T/2) = \bar{v}_1(t)$.
5. Traveling rolls: $v_2 = v_3 = 0$, $v_1 = V\exp(i\omega t)$.
6. Traveling patchwork quilt (1): $v_1 = V_1\exp(2i\omega t)$, $v_2 = v_3 = V_2\exp(-i\omega t)$.
7. Traveling patchwork quilt (2): $v_1 = V_1$ real, $v_2 = \bar{v}_3 = V_2\exp(i\omega t)$.
8. Oscillating triangles: $v_1 = v_2 = v_3$, $v_1(t + T/3) = \exp(2\pi i/3)v_1(t)$.
9. Twisted patchwork quilt: v_1 real, $v_2(t) = v_1(t + T/3)$, $v_3(t) = v_1(t + 2T/3)$.
10. Wavy rolls (2): $v_1(t + T/2) = \bar{v}_1(t)$, $v_2(t) = v_1(t + T/3)$, $v_3(t) = v_1(t + 2T/3)$.
11. Wavy rolls (1): v_1, v_2, v_3 real, $v_2(t) = -v_1(t + T/4)$, $v_1(t) = v_2(t + T/4)$, $v_3(t + T/4) = -v_3(t)$.

To look for periodic solutions of Eq. (15), we proceed in two steps. We first set $\epsilon = 0$ and look for periodic orbits of the Hamiltonian system. These will exist in one-parameter families (once we fix centers or axes of symmetry to eliminate the translation symmetries). When dissipation is added in ($\epsilon > 0$), only isolated solutions in each one-parameter family persist. In nondegenerate cases, persistence is determined by an integral condition requiring the average dissipation to be zero. For each periodic orbit of the Hamiltonian system, this yields a condition determining γ as a function of ϵ if the other coefficients are given.

Specifically, the condition for persistence of periodic orbits is obtained as follows (this discussion is analogous to Lemma 2.1, on p. 445 of [20]). With q_k defined as in the remark following Eq. (16), we can put Eq. (15) in the

form

$$\ddot{q}_k = -\frac{\partial V}{\partial q_k} + \epsilon F_k(q). \tag{17}$$

For $\epsilon = 0$, let $q^0(t)$ be a periodic solution with period T. If we then look for periodic solutions for small ϵ by a regular perturbation expansion, then the solvability condition

$$\int_0^T \sum_k \dot{q}_k^0(t) F_k(q^0(t))\,\mathrm{d}t = 0 \tag{18}$$

arises at the leading order. Since

$$F_k(q) = -2\gamma\dot{q}_k + \dots, \tag{19}$$

with the dot indicating terms which do not depend on γ, we can use Eq. (18) to solve for γ.

5.3. *Secondary bifurcation of periodic orbits from steady solutions*

We shall now look for branches of periodic solutions which bifurcate from steady solutions. We focus our analysis on the Hamiltonian system which is obtained by setting $\epsilon = 0$ in Eq. (15):

$$\begin{aligned}
&\ddot{v}_1 \mp v_1 + b_2\bar{v}_2\bar{v}_3 + c_4|v_1|^2 v_1 + c_7(|v_2|^2 + |v_3|^2)v_1 = 0,\\
&\ddot{v}_2 \mp v_2 + b_2\bar{v}_1\bar{v}_3 + c_4|v_2|^2 v_2 + c_7(|v_1|^2 + |v_3|^2)v_2 = 0,\\
&\ddot{v}_3 \mp v_3 + b_2\bar{v}_2\bar{v}_1 + c_4|v_3|^2 v_3 + c_7(|v_2|^2 + |v_1|^2)v_3 = 0.
\end{aligned} \tag{20}$$

For steady solutions, the system (20) is exactly the same which is found in the study of steady onset for the Bénard problem (without up–down symmetry, see [19]). With the equations truncated at the cubic level as in Eq. (20), there are three types of steady solutions: rolls, hexagons, and solutions with rectangular symmetry, which we shall refer to as steady patchwork quilt (they are called type IV solutions in [19]). The latter solutions do not bifurcate directly from the trivial state unless $b_2 = 0$, instead they form a secondary branch which connects rolls and hexagons.

5.3.1. *Bifurcation from steady rolls*

Steady rolls are given by $v_1 = V$, $v_2 = v_3 = 0$, where V is real and

$$\mp V + c_4 V^3 = 0. \tag{21}$$

The linearization of Eq. (20) at a steady roll solution leads to the problem (with y_i denoting the linearized perturbation to v_i)

$$\begin{aligned}
&\ddot{y}_1 + c_4 V^2(y_1 + \bar{y}_1) = 0,\\
&\ddot{y}_2 + b_2 V\bar{y}_3 + (c_7 - c_4)V^2 y_2 = 0,\\
&\ddot{y}_3 + b_2 V\bar{y}_2 + (c_7 - c_4)V^2 y_3 = 0.
\end{aligned} \tag{22}$$

We are interested in periodic solutions with a time dependence proportional to $\exp(\mathrm{i}\omega t)$. The eigenvalue problem for ω leads to the following eigenspaces:

1. $y_1 = -\bar{y}_1$, $y_2 = y_3 = 0$ and $\omega = 0$. This zero eigenvalue results from the translation symmetry of the problem, which allows for a translation of the steady rolls pattern. Associated with this translation symmetry, we have

traveling rolls bifurcating from the one-parameter family of steady rolls. We shall find traveling wave solutions explicitly in the next subsection.

The abstract situation for bifurcation of traveling waves is as follows: we have a system of equations of the form

$$\ddot{u} = F(u), \quad u \in \mathbb{R}^{2n}, \tag{23}$$

where F is invariant under an O(2)-symmetry, i.e. there is a group of rotation $\exp(L\tau)$ and a reflection R such that

$$F(\exp(L\tau)u) = \exp(L\tau)F(u), \qquad F(Ru) = RF(u), \qquad RL = -LR. \tag{24}$$

Let u_0 be a steady solution invariant under reflection, but not rotation, i.e. $Ru_0 = u_0$, $Lu_0 \neq 0$. The space $\mathbb{R}^{2n}$ can be decomposed into an even subspace ($Ru = u$) and an odd subspace ($Ru = -u$), both these subspaces are invariant under the Jacobian $DF(u_0)$. We have $DF(u_0)Lu_0 = 0$, and Lu_0 is in the odd subspace; generically, there are no null vectors of $DF(u_0)$ in the even subspace. Now look for solutions of Eq. (23) which are traveling waves, i.e. they have the form $\exp(\alpha Lt)v$, where α is a constant and v does not depend on t. We impose the additional condition that v is even: $Rv = v$. Then Eq. (23) yields

$$\alpha^2 L^2 v = F(v), \tag{25}$$

and the implicit function theorem yields a unique solution $v = v(\alpha^2)$ in a neighborhood of $\alpha = 0$, $v = u_0$.

2. $y_1 = \bar{y}_1$, $y_2 = y_3 = 0$ and $\omega^2 = 2c_4V^2$. If $c_4 > 0$, then there exists a family of periodic orbits of the Hamiltonian system, which are standing rolls, i.e. y_1 is real and $y_2 = y_3 = 0$. These standing rolls are not the standing rolls of [15], since they oscillate about a nonzero mean. In the analysis of [21], these are the standing rolls of type SW_3.
3. $y_1 = 0$, $y_2 = \bar{y}_3$ and $\omega^2 = b_2V + (c_7 - c_4)V^2$, This eigenspace is two-dimensional. We have an O(2) symmetry, with translation given by $y_2 \to y_2 \exp(\mathrm{i}\alpha)$, $y_3 \to y_3 \exp(-\mathrm{i}\alpha)$ and reflection given by exchange of y_2 and y_3. If $\omega^2 > 0$, the nonlinear problem will therefore allow for standing and traveling wave solutions (see [22], Chapter XVII). This leads to a family of periodic orbits which are standing patchwork quilts: $v_2 = v_3$ real, and a family of traveling patchwork quilts (2): $v_2(t + \tau) = \exp(\mathrm{i}\omega\tau)v_2(t)$.
4. $y_1 = 0$, $y_2 = -\bar{y}_3$ real and $\omega^2 = -b_2V + (c_7 - c_4)V^2$. This case is equivalent to the situation obtained when $y_2 = \bar{y}_3$ and the sign of V is reversed (note that Eq. (15) is invariant under simultaneous sign change of v_1 and v_3, and that this transformation can be interpreted as a translation). Hence the periodic orbits which exist for $\omega^2 > 0$ are again a family of standing patchwork quilts and a family of traveling patchwork quilts (2).

5.3.2. Secondary bifurcation from steady hexagons

Steady hexagons are given by $v_1 = v_2 = v_3 = V$, where V is real and

$$\mp V + b_2V^2 + (c_4 + 2c_7)V^3 = 0. \tag{26}$$

The linearization of Eq. (20) at a steady hexagon leads to the system

$$\begin{aligned}
&\ddot{y}_1 + b_2V(\bar{y}_2 + \bar{y}_3 - y_1) + c_4V^2(y_1 + \bar{y}_1) + c_7V^2(y_2 + \bar{y}_2 + y_3 + \bar{y}_3) = 0,\\
&\ddot{y}_2 + b_2V(\bar{y}_1 + \bar{y}_3 - y_2) + c_4V^2(y_2 + \bar{y}_2) + c_7V^2(y_1 + \bar{y}_1 + y_3 + \bar{y}_3) = 0,\\
&\ddot{y}_3 + b_2V(\bar{y}_2 + \bar{y}_1 - y_3) + c_4V^2(y_3 + \bar{y}_3) + c_7V^2(y_2 + \bar{y}_2 + y_1 + \bar{y}_1) = 0.
\end{aligned} \tag{27}$$

We have the following eigenspaces for the linearized problem and associated bifurcating branches:

1. $y_1 = y_2 = y_3$ real and $\omega^2 = b_2V + (2c_4 + 4c_7)V^2$. If $\omega^2 > 0$, there is a branch of standing hexagons.

2. $y_1 = y_2 = y_3$ imaginary and $\omega^2 = -3b_2V$. If $\omega^2 > 0$, this leads to a branch of standing regular triangles bifurcating from the steady hexagons.
3. y_1, y_2, y_3 imaginary and $y_1+y_2+y_3 = 0$. This leads to a double zero eigenvalue associated with the translation invariance of the problem. Associated with this double zero eigenvalue, we have bifurcating branches of both types of traveling patchwork quilt, see the next subsection.
4. y_1, y_2, y_3 real, $y_1 + y_2 + y_3 = 0$, and $\omega^2 = -2b_2V + 2c_4V^2 - 2c_7V^2$. If $\omega^2 > 0$, we can use the equivariant Hopf bifurcation theorem for systems with D_3-symmetry (see Theorem 4.1, p. 390 in [22]) to obtain the following types of bifurcating solutions:
   (a) Solutions for which two of the amplitudes, say v_2 and v_3 are equal. Such solutions have rectangular symmetry. They are a type of standing patchwork quilt, but not the standing patchwork quilts of [15], since they oscillate about a steady hexagon, so all amplitudes have nonzero mean.
   (b) Solutions for which $v_2(t) = v_1(t+T/3),\ v_3(t) = v_1(t+2T/3)$. In the linearized problem, these solutions are given by $y_1 = \cos(\omega t)$, $y_2 = \cos(\omega t + 2\pi/3)$, $y_3 = \cos(\omega t + 4\pi/3)$. These solutions are twisted patchwork quilts.
   (c) Solutions for which $v_2(t+T/2) = v_3(t),\ v_3(t+T/2) = v_2(t)$ and $v_1(t+T/2) = v_1(t)$. In the linearized problem, such a solution is given by $y_2 = -y_3,\ y_1 = 0$. The spatial patterns on this solution branch have point symmetry across the origin (since v_1, v_2 and v_3 are real). Moreover, shift by half a temporal period is equivalent to reflection across the x-axis (i.e., exchange of v_2 and v_3).

5.3.3. Secondary bifurcation from steady patchwork quilts

Steady patchwork quilts are given by $v_1 = U$, $v_2 = v_3 = V$, where U and V are real and

$$\mp U + b_2V^2 + c_4U^3 + 2c_7V^2U = 0, \qquad \mp V + b_2UV + c_4V^3 + c_7(U^2+V^2)V = 0. \tag{28}$$

If we exclude the case of rolls ($V = 0$), we can divide the second equation by V and obtain

$$\mp 1 + b_2U + c_4V^2 + c_7(U^2+V^2) = 0. \tag{29}$$

Next, we subtract the two equations in (28) from each other and divide by $U - V$ (the case $U = V$ leads to hexagons). The result is

$$\mp 1 - b_2V + c_4(U^2 + UV + V^2) + c_7(V^2 - UV) = 0. \tag{30}$$

Next, we subtract Eq. (30) from Eq. (29) and divide by $U + V$ (the case $U + V = 0$ also leads to hexagons). The result is

$$U = \frac{b_2}{c_4 - c_7}. \tag{31}$$

From Eq. (29), we then find

$$(c_4 + c_7)V^2 = \pm 1 - \frac{c_4b_2^2}{(c_4 - c_7)^2}. \tag{32}$$

The equations for linearized perturbations are

$$\begin{aligned}
&\ddot{y}_1 \mp y_1 + b_2V(\bar{y}_2 + \bar{y}_3) + c_4U^2(2y_1 + \bar{y}_1) + 2c_7V^2y_1 + c_7UV(y_2 + \bar{y}_2 + y_3 + \bar{y}_3) = 0,\\
&\ddot{y}_2 \mp y_2 + b_2(U\bar{y}_3 + V\bar{y}_1) + c_4V^2(2y_2 + \bar{y}_2) + c_7(U^2+V^2)y_2 + c_7UV(y_1 + \bar{y}_1) + c_7V^2(y_3 + \bar{y}_3) = 0,\\
&\ddot{y}_3 \mp y_3 + b_2(U\bar{y}_2 + V\bar{y}_1) + c_4V^2(2y_3 + \bar{y}_3) + c_7(U^2+V^2)y_3 + c_7UV(y_1 + \bar{y}_1) + c_7V^2(y_2 + \bar{y}_2) = 0.
\end{aligned} \tag{33}$$

We can identify the following eigenspaces

1. $y_1,\ y_2,\ y_3$ imaginary, $y_2 = y_3,\ y_1 = -2Uy_2/V,\ \omega^2 = 0$. This zero eigenvalue is associated with the translation symmetry in the x-direction. Associated with this symmetry, we have a bifurcation of traveling patchwork quilts (1).
2. $y_2,\ y_3$ imaginary, $y_2 = -y_3,\ y_1 = 0, ,\omega^2 = 0$. This zero eigenvalue is associated with the translation symmetry in the y-direction. Associated with this translation symmetry, there is a bifurcating branch of traveling patchwork quilts (2).
3. $y_1,\ y_2,\ y_3$ imaginary, $y_2 = y_3,\ y_1 = Vy_2/U,\ \omega^2 = b_2(2U + V^2/U)$. A branch of periodic solutions exists if $\omega^2 > 0$. These periodic solutions retain symmetry across the x-axis, i.e. $v_2 = v_3$, but they become reflected across the y-axis every half period: $v_1(t + T/2) = \bar{v}_1(t),\ v_2(t + T/2) = \bar{v}_3(t),\ v_3(t + T/2) = \bar{v}_2(t)$.
4. $y_1,\ y_2,\ y_3$ real, $y_2 = -y_3,\ y_1 = 0,\ \omega^2 = \mp 1 - b_2U + 3c_4V^2 + c_7(U^2 - V^2)$. This leads to branches of periodic solutions which preserve point symmetry across the origin, but become reflected across the axes every half period: $v_1(t + T/2) = v_1(t)$, $v_2(t + T/2) = v_3(t)$, $v_3(t + T/2) = v_2(t)$.
5. $y_1,\ y_2,\ y_3$ real, $y_2 = y_3$. Such solutions preserve the rectangular symmetry. The linearized eigenvalue problem is two-dimensional:

$$\begin{aligned} &-\omega^2 y_1 \mp y_1 + 2b_2Vy_2 + 3c_4U^2y_1 + 2c_7V^2y_1 + 4c_7UVy_2 = 0,\\ &-\omega^2 y_2 \mp y_2 + b_2(Uy_2 + Vy_1) + 3c_4V^2y_2 + c_7(U^2y_2 + 2UVy_1 + 3V^2y_2) = 0. \end{aligned} \tag{34}$$

In general, there are two different eigenvalues for ω^2, and branches of periodic solutions exist if one or both of these eigenvalues are positive. The patterns resulting from this are standing patchwork quilts with nonzero mean, analogous to those which we found bifurcating from steady hexagons.

5.4. Traveling waves

We can identify two types of traveling waves (other than rolls), corresponding to the two types of traveling patchwork quilts in [15]. For the first kind of traveling wave, v_1 is real and time-independent, and $v_2 = \bar{v}_3$ is complex and has a time dependence proportional to $e^{i\omega t}$:

$$v_1 = V_1, \qquad v_2 = V_2e^{i\omega t}, \qquad v_3 = \bar{V}_2e^{-i\omega t}.$$

This type of traveling wave corresponds to the traveling patchwork quilt (2) in [15] and to the traveling wave of type C2 in [10]. For the present case, we obtain the algebraic system

$$\begin{aligned} &\mp V_1 + b_2|V_2|^2 + c_4V_1^3 + 2c_7|V_2|^2V_1 = 0,\\ &-\omega^2V_2 \mp V_2 + b_2V_1V_2 + c_4|V_2|^2V_2 + c_7(|V_2|^2 + V_1^2)V_2 = 0. \end{aligned} \tag{35}$$

We divide the second equation by V_2, and solve for $|V_2|^2$:

$$|V_2|^2 = \frac{\omega^2 \pm 1 - b_2V_1 - c_7V_1^2}{c_4 + c_7} > 0. \tag{36}$$

We can now insert this result in the first equation of (35), leading to a cubic equation for V_1. We note that this type of traveling wave becomes a steady roll when $V_2 = 0$. See also the discussion of secondary bifurcations from steady rolls above.

The second type of traveling wave corresponds to the traveling patchwork quilt (1) of [15] and the traveling waves of type D of [10]. For these solutions, we have

$$v_1 = V_1e^{i\omega t}, \qquad v_2 = v_3 = V_2e^{-i\omega t/2}. \tag{37}$$

We obtain the algebraic system

$$-\omega^2 V_1 \mp V_1 + b_2 \bar{V}_2^2 + c_4 |V_1|^2 V_1 + 2c_7 |V_2|^2 V_1 = 0,$$

$$-\frac{\omega^2}{4} V_2 \mp V_2 + b_2 \bar{V}_1 \bar{V}_2 + c_4 |V_2|^2 V_2 + c_7 (|V_2|^2 + |V_1|^2) V_2 = 0. \tag{38}$$

We multiply the first equation by $\bar{V}_1$, and the second by $\bar{V}_2$, resulting in

$$-\omega^2 |V_1|^2 \mp |V_1|^2 + b_2 \bar{V}_2^2 \bar{V}_1 + c_4 |V_1|^4 + 2c_7 |V_2|^2 |V_1|^2 = 0,$$

$$-\frac{\omega^2}{4} |V_2|^2 \mp |V_2|^2 + b_2 \bar{V}_1 \bar{V}_2^2 + c_4 |V_2|^4 + c_7 (|V_2|^2 + |V_1|^2) |V_2|^2 = 0. \tag{39}$$

If $b_2 \neq 0$, we conclude that $V_2^2 V_1$ must be real. We set $r_1 = \pm |V_1|,\ \rho_2 = |V_2|^2$, with the sign chosen such that $\bar{V}_1 \bar{V}_2^2 = r_1 \rho_2$. After dividing the first equation of (39) by r_1 and the second by ρ_2, we find

$$-\omega^2 r_1 \mp r_1 + b_2 \rho_2 + c_4 r_1^3 + 2c_7 \rho_2 r_1 = 0,$$

$$-\frac{\omega^2}{4} \mp 1 + b_2 r_1 + c_4 \rho_2 + c_7 (\rho_2 + r_1^2) = 0. \tag{40}$$

We solve the second equation for ρ_2:

$$\rho_2 = \frac{(\omega^2/4) \pm 1 - b_2 r_1 - c_7 r_1^2}{c_4 + c_7} > 0. \tag{41}$$

By inserting Eq. (41) into the first equation of (40), we obtain a third-degree equation in r_1. This type of traveling wave becomes a traveling roll when $\rho_2 = 0$.

We note that if we set $\omega = 0$ for either type of traveling patchwork quilt, we recover the steady patchwork quilts.

5.5. *Heteroclinic orbits*

We can expect a multitude of solutions with more complicated time dependence than periodicity. For instance, the Hamiltonian system for $\epsilon = 0$ will have many invariant tori, and if we include the dissipation, we can expect some of these tori to persist, leading to quasiperiodic solutions. Dangelmayr and Knobloch [21] identified such a family of quasiperiodic solutions for the case of rolls. In the numerical results of the next section, we shall indeed see some quasiperiodic regimes, as well as chaotic ones.

For the simple cases of rolls and hexagons, the Hamiltonian system can be integrated, and it is easy to see that homoclinic or heteroclinic orbits exist as limiting cases of periodic solutions. Although many such solutions are expected to exist in other symmetry classes, it is not possible to obtain the global dynamics of the Hamiltonian system from direct integration. We shall show indirectly that a heteroclinic connection between steady hexagons arises as a limit of oscillating triangles if $b_2 \neq 0$ and $c_4 + 2c_7 < 0$. Let us consider solutions with triangular symmetry, i.e., $v_1 = v_2 = v_3$. In this case, our Hamiltonian system reduces to:

$$\ddot{v} \mp v + b_2 \bar{v}^2 + (c_4 + 2c_7) |v|^2 v = 0. \tag{42}$$

If we choose the plus sign, there is a family of oscillating triangles bifurcating from the origin. By the global Hopf bifurcation theorem [17,23], this family of periodic solutions must either grow unbounded, reach a bifurcation point from another steady solution, or else the period must tend to infinity. Since oscillating triangles have zero average,

bifurcation from a steady solution other than the origin is impossible. Next, we show that the family of oscillating triangles cannot be unbounded.

We rewrite v in terms of its real and imaginary parts: $v = x + \mathrm{i}y$. We also introduce the 'momentum' variables $p = \dot{x}$ and $q = \dot{y}$. The equation of motion is then $\dot{x} = \partial H/\partial p,\ \dot{y} = \partial H/\partial q,\ \dot{p} = -\partial H/\partial x,\ \dot{q} = -\partial H/\partial y$, and the Hamiltonian is

$$H = \tfrac{1}{2}(p^2 + q^2 + x^2 + y^2) + b_2(\tfrac{1}{3}x^3 - xy^2) + \tfrac{1}{4}(c_4 + 2c_7)(x^2 + y^2)^2.$$

Consider now the potential part of the energy

$$U = \tfrac{1}{2}(x^2 + y^2) + b_2(\tfrac{1}{3}x^3 - xy^2) + \tfrac{1}{4}(c_4 + 2c_7)(x^2 + y^2)^2.$$

We have

$$\dot{U} = \frac{\partial U}{\partial x}p + \frac{\partial U}{\partial y}q,$$

$$\ddot{U} = \frac{\partial U}{\partial x}\dot{p} + \frac{\partial U}{\partial y}\dot{q} + \frac{\partial^2 U}{\partial x^2}p^2 + 2\frac{\partial^2 U}{\partial x \partial y}pq + \frac{\partial^2 U}{\partial y^2}q^2.$$

Using the equation of motion, we find

$$\ddot{U} = -\dot{p}^2 - \dot{q}^2 + \frac{\partial^2 U}{\partial x^2}p^2 + 2\frac{\partial^2 U}{\partial x \partial y}pq + \frac{\partial^2 U}{\partial y^2}q^2. \tag{43}$$

If $c_4 + 2c_7 < 0$, then U is negative and concave for large $x^2 + y^2$. This means that the expression in Eq. (43) is also negative if $x^2 + y^2$ is large. However, at a minimum of U along a periodic solution, $\ddot{U}$ must be positive. This means that, along every periodic solution, we obtain a priori bound for $x^2 + y^2$ at the point where U has its minimum, and consequently, everywhere. The a priori bounds for $|x|$ and $|y|$ yield a priori bounds for $|\ddot{x}|$ and $|\ddot{y}|$ by means of the equation of motion, and a priori bounds for the first derivatives follow by the identity

$$\dot{x}(t) = x(t+1) - x(t) - \int_t^{t+1}\int_t^{\tau} \ddot{x}(s)\,\mathrm{d}s\,\mathrm{d}\tau.$$

Consequently, the family of oscillating triangles cannot be unbounded.

Therefore, there must be a family of oscillating triangle solutions for which the period tends to infinity. We shall now show that this necessarily implies a heteroclinic connection between hexagons. For this, we set $v = r\exp(\mathrm{i}\phi)$ in Eq. (42), and we obtain

$$\ddot{r} - r\dot{\phi}^2 + r + b_2 r^2\cos(3\phi) + (c_4 + 2c_7)r^3 = 0,$$

$$r\ddot{\phi} + 2\dot{r}\dot{\phi} - b_2 r^2\sin(3\phi) = 0. \tag{44}$$

For oscillating triangles close to the bifurcation from the origin, ϕ is clearly an increasing function of t. We claim that there is a global family of oscillating triangles such that

(a) r is never zero and ϕ is increasing monotonically with time.

(b) $v(t)$ winds around the origin once during one period.

We note that as long as (a) holds, a winding number is well-defined. Since this winding number is a topological invariant, it remains constant along a continuous family of solutions. Now suppose that (a) fails at some point. Then either $v(t)$ must cross the origin or $\dot{\phi}$ must become zero at some point. If $v(t)$ crosses the origin, it must do so at least three times in three different directions, due to the spatio-temporal symmetry of oscillating triangles

Table 5
List of coefficients b_i, $\tilde{b}_i$, c_i, $\tilde{c}_i$ of Eqs. (11) and (12) in (a) the Anderinert/silicone oil system, (b) Fluorinert/silicone oil system, (c) those of [17]. The values of l_1 and coefficients of the last column are given to two decimal places. The coefficients of the last column is given to four places in order to distinguish c_8 and c_{10}

	(a)		(b)	(c)	
l_1	0.48	0.51	0.423	0.52	0.48303
b_2	14.613	5.24	−5.79	−4.11	−0.76
b_3	−1.079	−0.34	1.26	0.97	−0.081
c_3	−1.489	1.17	−0.86	3.1	0.0036
c_4	11.584	−8.85	−0.78	−5.4	0.023
c_5	−0.738	1.29	−0.004	2.4	0.0017
c_7	12.855	−9.79	−2.96	−4.95	0.027
c_8	−0.706	−0.02	0.62	0.82	0.0025
c_9	−0.425	1.52	1.97	2.58	0.0033
c_{10}	−0.715	1.48	0.06	2.63	0.0023
$\tilde{b}_2$	1.000	−0.08	−0.42	−0.36	0.082
$\tilde{c}_4$	3.010	1.57	1.59	0.21	0.0010
$\tilde{c}_7$	3.736	2.00	1.94	0.59	0.0015

$(v(t+T/3) = v(t)\exp(2\pi \mathrm{i}/3))$. Such a solution cannot be a limit of simple loops. If $\dot{\phi}$ becomes zero at some point, while $\dot{\phi} \geq 0$ elsewhere, then necessarily $\ddot{\phi} = 0$ at the same point. From Eq. (44), we infer that then necessarily $\sin(3\phi) = 0$ and ϕ is a constant independent of time. The orbit would therefore contain a straight line segment, which is also impossible.

The only possibility left is that the period tends to infinity because the solution comes close to a steady solution. Since the only steady solutions with triangular symmetry are hexagons, this implies the existence of heteroclinic orbits between hexagons as claimed.

6. Numerical results

Table 1 gives the physical parameters for each of the three systems we examine: Anderinert/silicone oil, Fluorinert/silicone oil and Fig. 2 of [4]. Tables 2–4 give further numerical data on the Takens–Bogdanov points. The corresponding coefficients b_i, $\tilde{b}_i$, c_i, $\tilde{c}_i$ of Eqs. (11) and (12) are listed in Table 5 We note that for the systems a and c we have listed values for two different Takens–Bogdanov points; these two points are on opposite ends of the 'window' in parameter space where Hopf bifurcations occur. That is, for values of l_1 in between these two extremes, complex conjugate eigenvalues occur, while the eigenvalues are real for values of l_1 outside this interval.

The analysis of Sections 5.2, 5.3, 5.4 and 5.5 concerns case B of Section 5.1.2, i.e., the case where the coefficients of the quadratic terms vanish. In the actual physical systems, the coefficients of the quadratic terms have some finite value so that for extremely small solutions, the cubics are small compared with quadratics and case A is appropriate. For this case, numerical calculations revealed no stable patterns of very small amplitudes. For more moderate amplitudes that may be physically realizable, numerical simulations are based directly on Eqs. (11) and (12), together with those coefficients which enter into case B and are tabulated in Table 5. Although we cannot justify this procedure rigorously, we expect it to have at least qualitative validity for our situation. We note that the analysis of case B assumed that the terms involving b_2, c_4 and c_7 are the dominant ones, and indeed the table shows numerical values of these particular coefficients which are large relative to the others.

For the numerical simulations reported below, we integrated the differential equations with a fourth-order Runge–Kutta scheme. We chose $\epsilon_1 = -0.1$, so that the trivial solution is always unstable, and we varied ϵ_2.

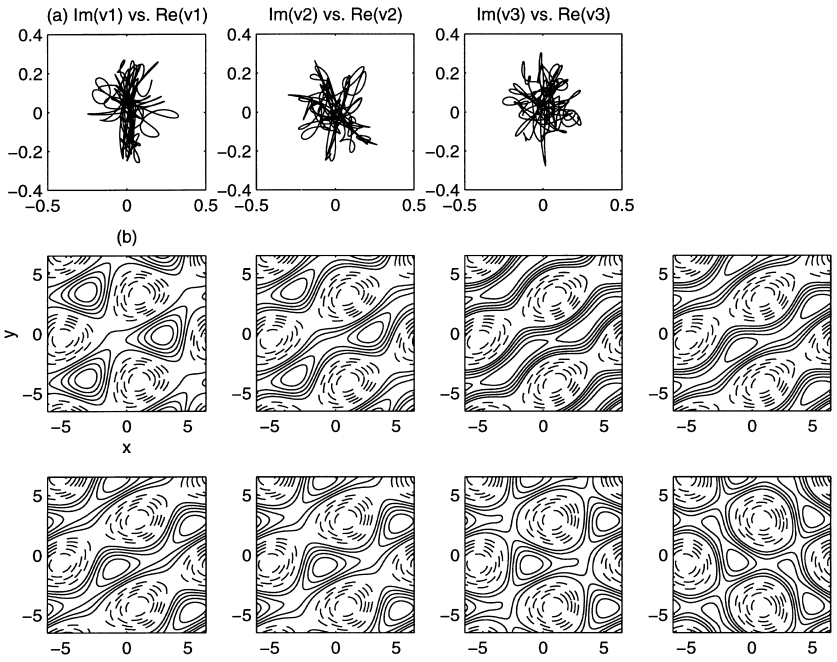

Fig. 9. (a) Temporal evolution of v_1, v_2 and v_3 for the data of Case (a), column 1, Table 5 and $\epsilon_2 = -1.5$. The real and imaginary parts of v_i are shown. (b) Spatial evolution for the data of Case (a), column 1, Table 5, and $\epsilon_2 = -1.5$. The patterns are in the (x–y) plane. Here, and in the subsequent plots, positive contour lines are solid, and negative contour lines are dashed. The sequence in all plots is spaced in time intervals of 0.2, left to right.

The initial condition was chosen to be small and without any particular symmetry; specifically, we chose the initial data $v_1 = 0.02,\ v_2 = 0.04,\ v_3 = 0.01 + 0.01\mathrm{i}$ and $w_1 = w_2 = w_3 = 0$. We then observed the long time behavior of the numerical solution which evolves from these initial data.

For all the data of Table 5, we see a general trend from steady to chaotic to quasiperiodic to periodic solutions as ϵ_2 is decreased. Specifically, we found the following behaviors:

Case (a), column 1:

Summary. For $\epsilon_2 \geq 1.5$, solutions become infinite in finite time. For $1.4 \geq \epsilon_2 \geq -1.4$, steady hexagons are observed. For $-1.5 \geq \epsilon_2 \geq -4.4$, we observe chaotic, then quasiperiodic solutions, which we shall describe in more detail below. At $\epsilon_2 = -4.5$, we find a periodic solution; in the terminology of [15], this solution is a traveling patchwork quilt (1). For $\epsilon \leq -4.6$, we find traveling rolls.

Specifics. We now show more details of the observed patterns in the chaotic and quasiperiodic regimes. In Figs. 9–18, we show the temporal and spatial evolution of patterns for $\epsilon_2 = -1.5, -1.8, -2.1, -2.7, -3.2, -3.5, -3.8, -4.0, -4.4$ and -4.5. In all cases, the first figure shows the temporal evolution of the amplitudes v_1, v_2 and v_3 in the complex plane as a function of time. The second figure shows a sequence of the corresponding spatial patterns; the plots are the level curves of $v_1\exp(\mathrm{i}x) + v_2\exp(-\mathrm{i}x/2 + \mathrm{i}\sqrt{3}y/2) + v_3\exp(-\mathrm{i}x/2 - \mathrm{i}\sqrt{3}y/2)$. The sequence of pictures, left to right, is spaced in time intervals of 0.2. The spatio-temporal evolution for this range of ϵ_2 is complicated, but some general trends can be noted. The temporal evolution is very irregular at $\epsilon_2 = -1.5$, and as ϵ_2 decreases, it gradually becomes more regular. At the same time, spatial patterns change from a regime dominated by triangles to one dominated by rolls. For ϵ_2 in the range from -2.1 to -3.5 (Figs. 11–14), the temporal pattern appears to be a chaotic perturbation of a quasiperiodic solution. We also note that the temporal evolution of two of the components v_i is very similar (e.g., v_1 and v_3 in Fig. 11 (a)), while the third one is completely different.

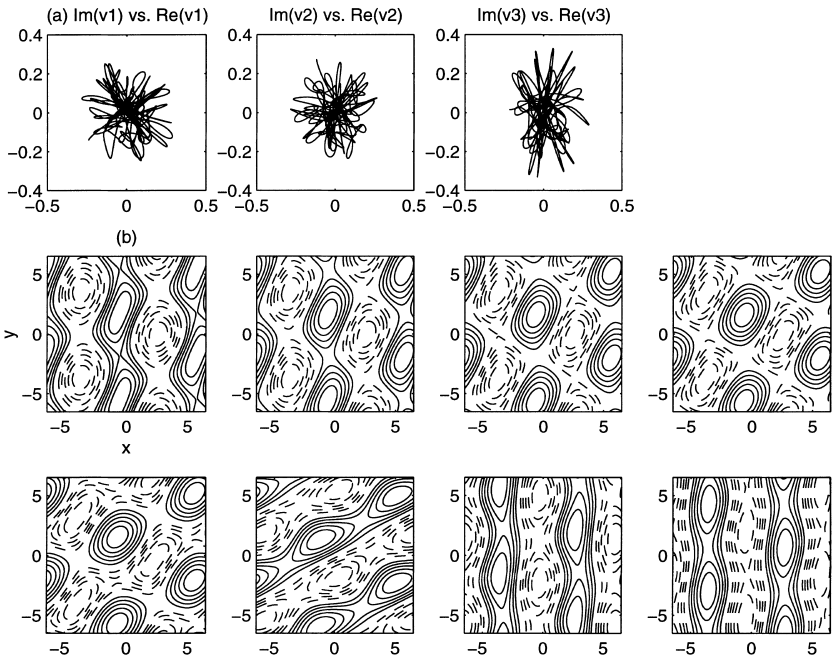

Fig. 10. (a) Temporal evolution of v_1, v_2 and v_3 for the data of Case (a), column 1, Table 5, and $\epsilon_2 = -1.8$. (b) Spatial evolution for the data of Case (a), column 1, Table 5, and $\epsilon_2 = -1.8$.

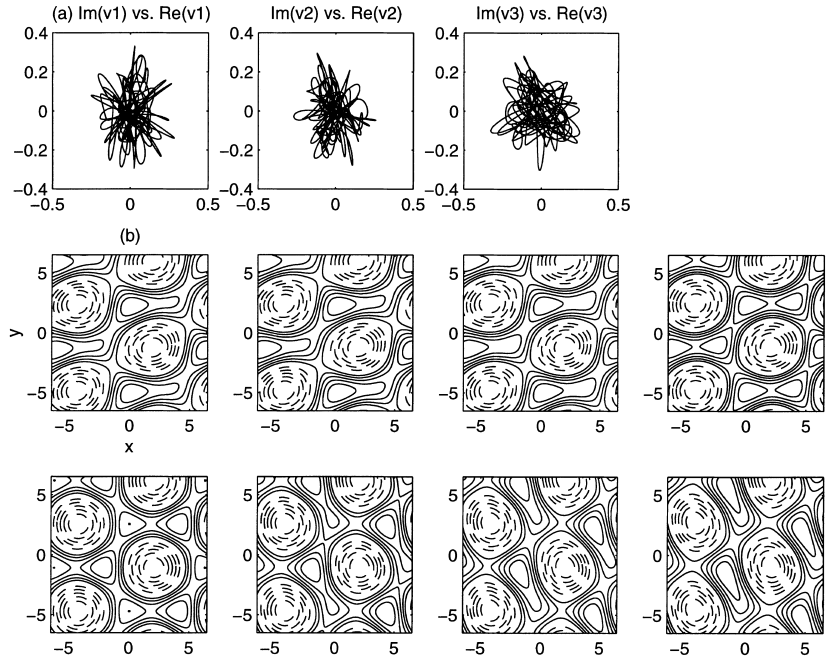

Fig. 11. (a) Temporal evolution of v_1, v_2 and v_3 for the data of Case (a), column 1, Table 5, and $\epsilon_2 = -2.1$. (b) Spatial evolution for the data of Case (a), column 1, Table 5, and $\epsilon_2 = -2.1$.

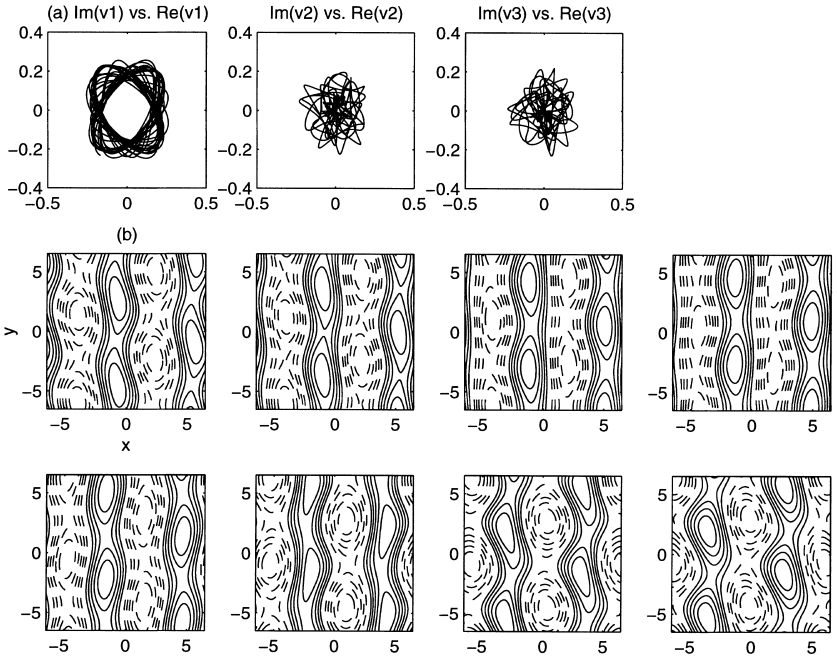

Fig. 12. (a) Temporal evolution of v_1, v_2 and v_3 for the data of Case (a), column 1, Table 5, and $\epsilon_2 = -2.7$. (b) Spatial evolution for the data of Case (a), column 1, Table 5, and $\epsilon_2 = -2.7$.

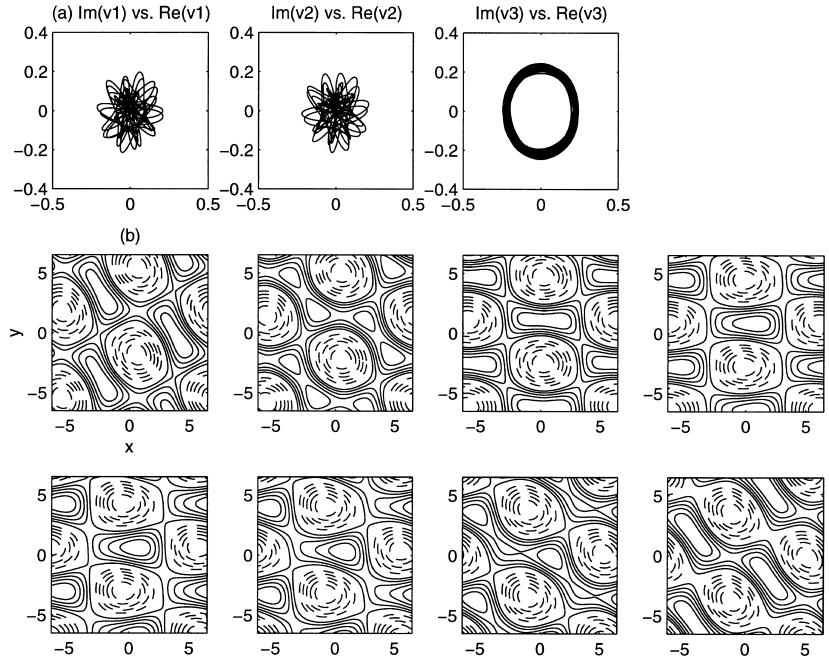

Fig. 13. (a) Temporal evolution of v_1, v_2 and v_3 for the data of Case (a), column 1, Table 5, and $\epsilon_2 = -3.2$. (b) Spatial evolution for the data of Case (a), column 1, Table 5, and $\epsilon_2 = -3.2$.

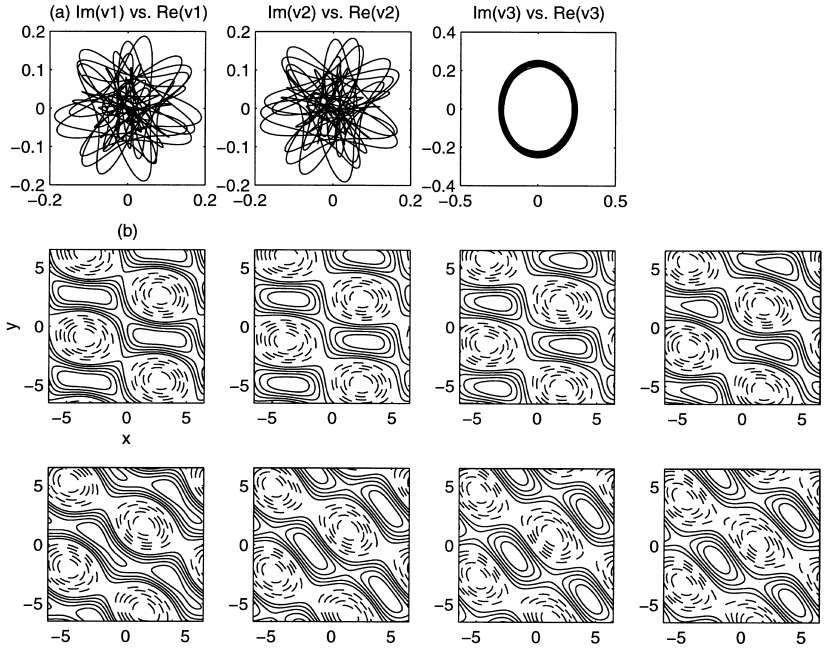

Fig. 14. (a) Temporal evolution of v_1, v_2 and v_3 for the data of Case (a), column 1, Table 5, and $\epsilon_2 = -3.5$. (b) Spatial evolution for the data of Case (a), column 1, Table 5, and $\epsilon_2 = -3.5$.

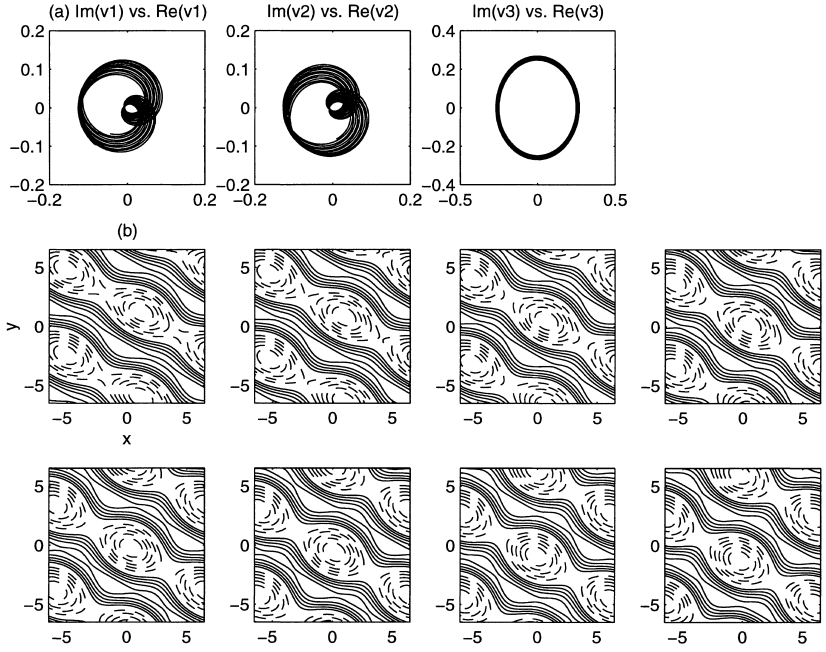

Fig. 15. (a) Temporal evolution of v_1, v_2 and v_3 for the data of Case (a), column 1, Table 5, and $\epsilon_2 = -3.8$. (b) Spatial evolution for the data of Case (a), column 1, Table 5, and $\epsilon_2 = -3.8$.

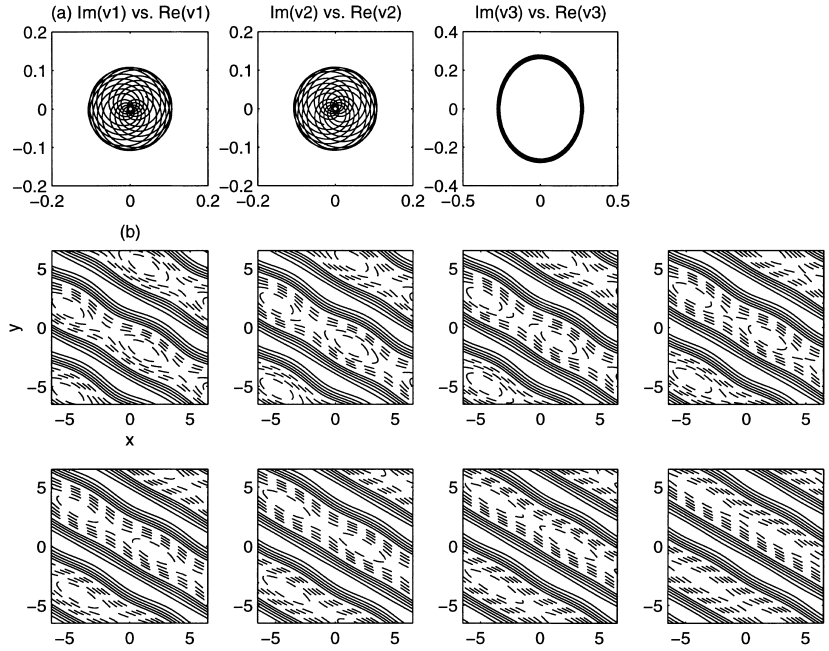

Fig. 16. (a) Temporal evolution of v_1, v_2 and v_3 for the data of Case (a), column 1, Table 5, and $\epsilon_2 = -4.0$. (b) Spatial evolution for the data of Case (a), column 1, Table 5, and $\epsilon_2 = -4.0$.

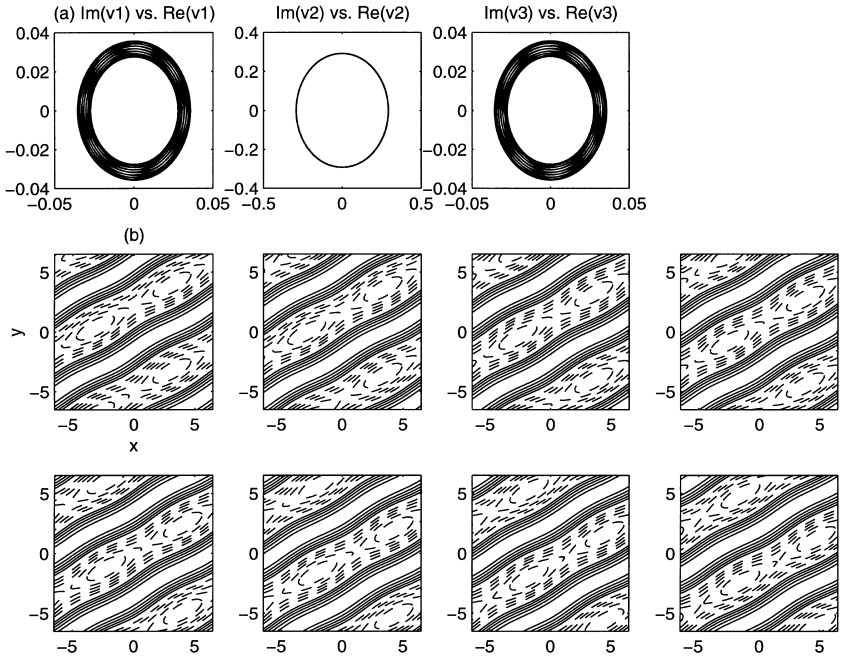

Fig. 17. (a) Temporal evolution of v_1, v_2 and v_3 for the data of Case (a), column 1, Table 5, and $\epsilon_2 = -4.4$. (b) Spatial evolution for the data of Case (a), column 1, Table 5, and $\epsilon_2 = -4.4$.

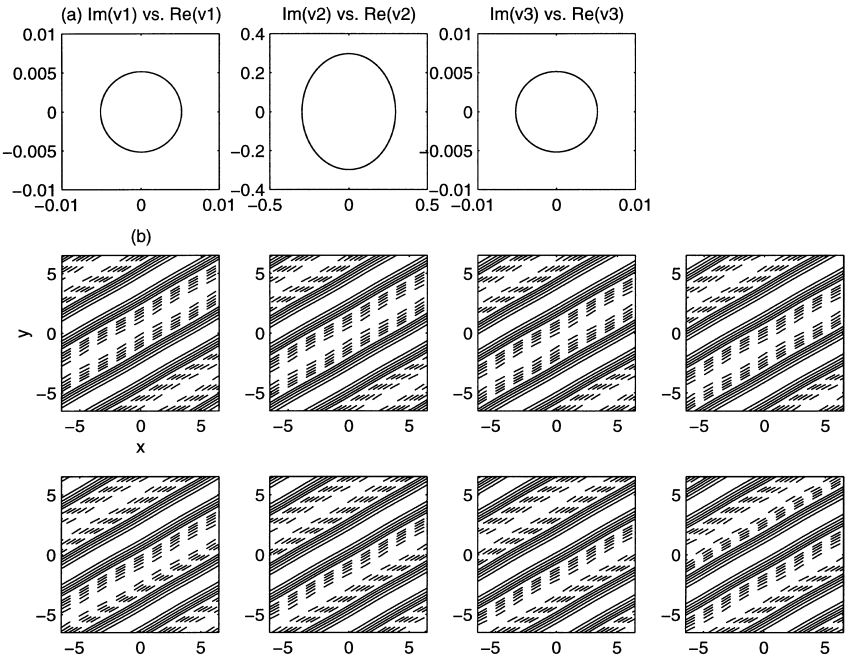

Fig. 18. (a) Temporal evolution of v_1, v_2 and v_3 for the data of Case (a), column 1, Table 5, and $\epsilon_2 = -4.5$. (b) Spatial evolution for the data of Case (a), column 1, Table 5, and $\epsilon_2 = -4.5$.

For $\epsilon_2 \leq -3.8$ (Figs. 15–17), the motion becomes quasiperiodic. It changes to a periodic motion at $\epsilon = -4.5$ (Fig. 18(a)). This periodic solution is a traveling patchwork quilt (1), in the terminology of [15]. The fact that such a solution is observed is somewhat remarkable, because the analysis of the Hopf bifurcation in [15] shows that the traveling patchwork quilt (1) is never stable near the bifurcation from the rest state. Of course, in the current situation, we do not see the traveling patchwork quilt (1) near a bifurcation from the rest state, but near a bifurcation from traveling rolls as discussed in the analysis of the preceding section.

Case (a), column 2:

Summary. Here we find steady rolls for $\epsilon_2 \geq 5.7$, steady hexagons for $5.6 \geq \epsilon_2 \geq -3.5$, chaotic solutions for $-3.6 \geq \epsilon_2 \geq -3.7$, and wavy rolls (1) for $\epsilon_2 \leq -3.8$.

Specifics. Figs. 19(a,b) show the spatio-temporal evolution for $\epsilon_2 = -3.6$, and Figs. 20(a,b) show $\epsilon_2 = -3.8$. The solution for $\epsilon_2 = -3.6$ is temporally chaotic, while the spatial pattern has the appearance of wavy rolls (1). The solution for $\epsilon_2 = -3.8$ is the temporally periodic wavy rolls (1).

Case (b):

Summary. This is the only case where no steady regime was found. We have blow-up in finite time for $\epsilon_2 \geq -1.8$, and a chaotic regime for $-1.9 \geq \epsilon_2 \geq -2.3$. For $-2.4 \geq \epsilon_2 \geq -2.6$, we find solutions which are temporally chaotic but have a triangular spatial symmetry. For $-2.7 \geq \epsilon_2 \geq -3$ and again for $\epsilon_2 \leq -4$, we have oscillating triangles. In the intervening interval, we have a traveling patchwork quilt (1) for $-3.1 \geq \epsilon_2 \geq -3.9$.

Specifics. Figs. 21–24 show patterns found at $\epsilon_2 = -2.1$, -2.5, -2.7 and -3.2. At $\epsilon_2 = -2.1$, we have a temporally chaotic solution, with an approximate but not exact triangular symmetry in the spatial pattern. At $\epsilon_2 = -2.5$, the temporal evolution is still chaotic, but the spatial pattern now has triangular symmetry and looks very much like oscillating triangles. At $\epsilon_2 = -2.7$, we find the temporally periodic oscillating triangles solution. We note the distinct triangular shape of the periodic orbits in Fig. 23(b). This, and the appearance of chaotic solutions

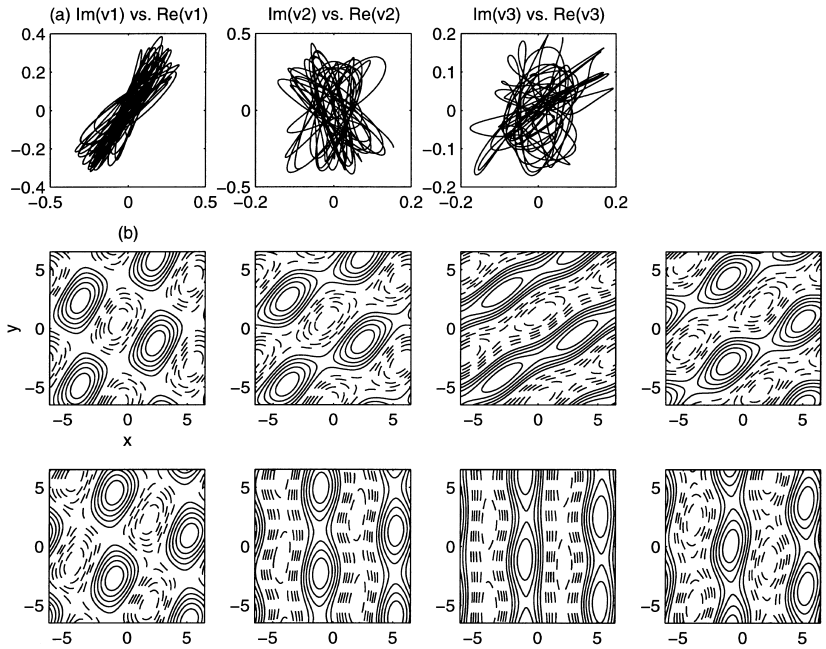

Fig. 19. (a) Temporal evolution of v_1, v_2 and v_3 for the data of Case (a), column 2, Table 5, and $\epsilon_2 = -3.6$. (b) Spatial evolution for the data of Case (a), column 2, Table 5 and $\epsilon_2 = -3.6$.

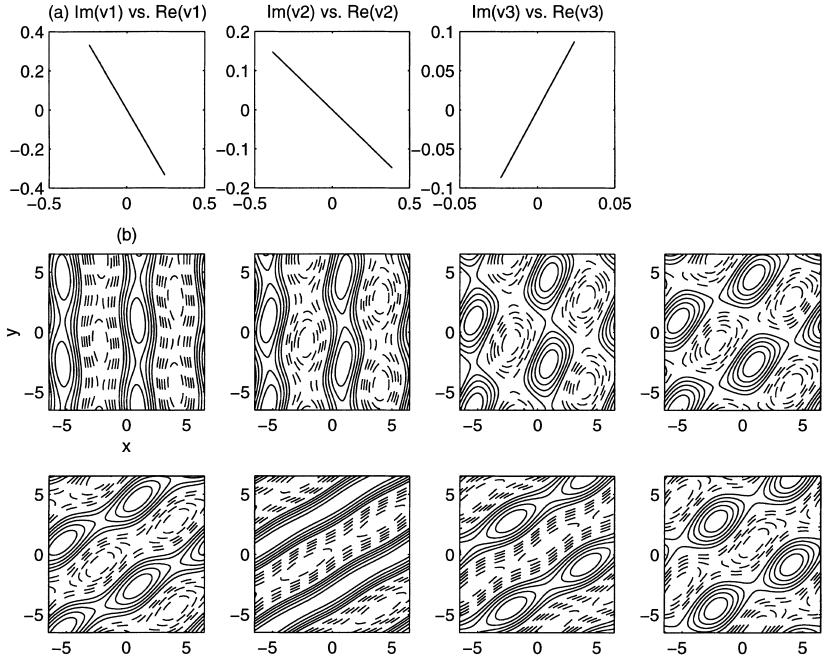

Fig. 20. (a) Temporal evolution of v_1, v_2 and v_3 for the data of Case (a), column 2, Table 5, and $\epsilon_2 = -3.8$. (b) Spatial evolution for the data of Case (a), column 2, Table 5, and $\epsilon_2 = -3.8$.

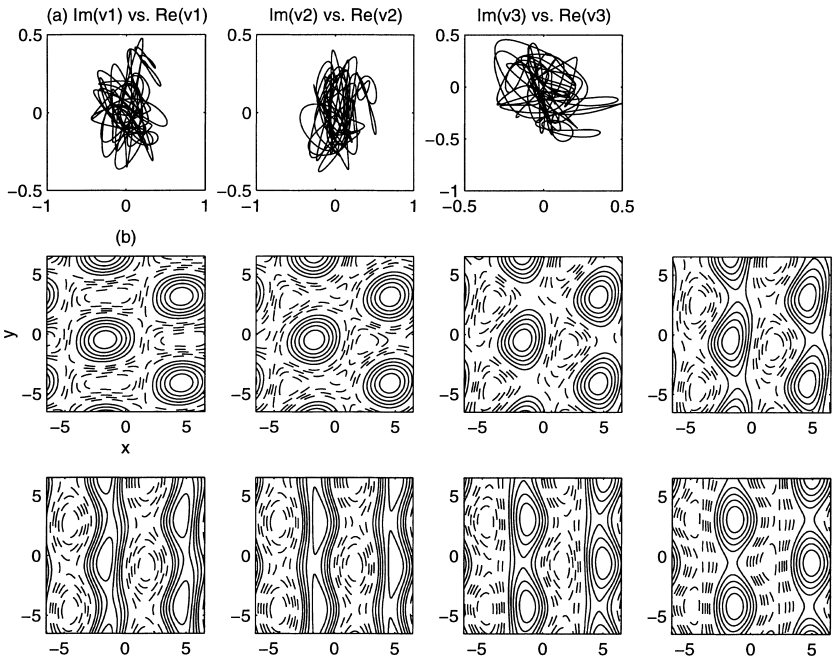

Fig. 21. (a) Temporal evolution of v_1, v_2 and v_3 for Fluorinert/silicone oil, Case (b) of Table 5, and $\epsilon_2 = -2.1$. (b) Spatial evolution for the data of Fluorinert/silicone oil, Case (b), Table 5, and $\epsilon_2 = -2.1$.

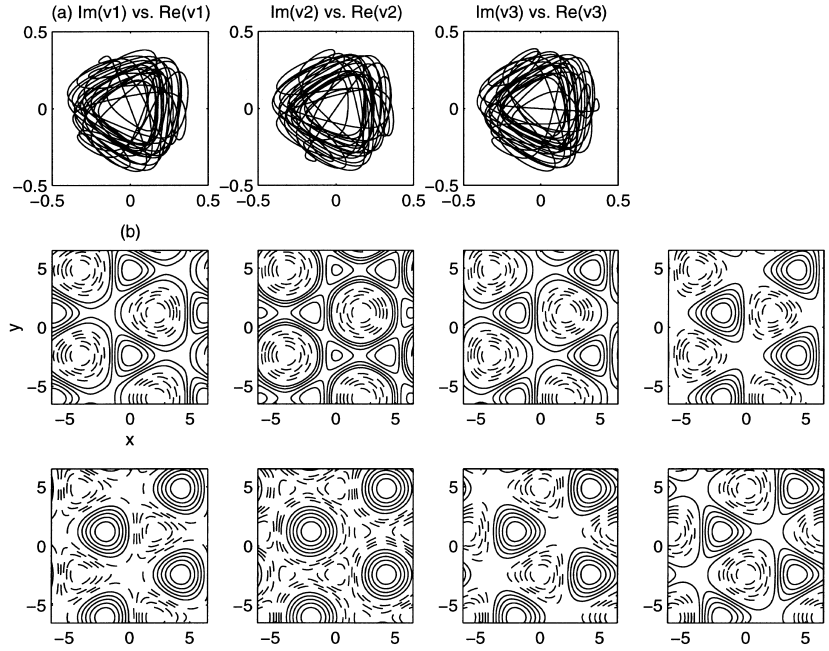

Fig. 22. (a) Temporal evolution of v_1, v_2 and v_3 for the data of Fluorinert/silicone oil, Case (b) of Table 5, and $\epsilon_2 = -2.5$. (b) Spatial evolution for Fluorinert/silicone oil, Case (b) of Table 5, and $\epsilon_2 = -2.5$.

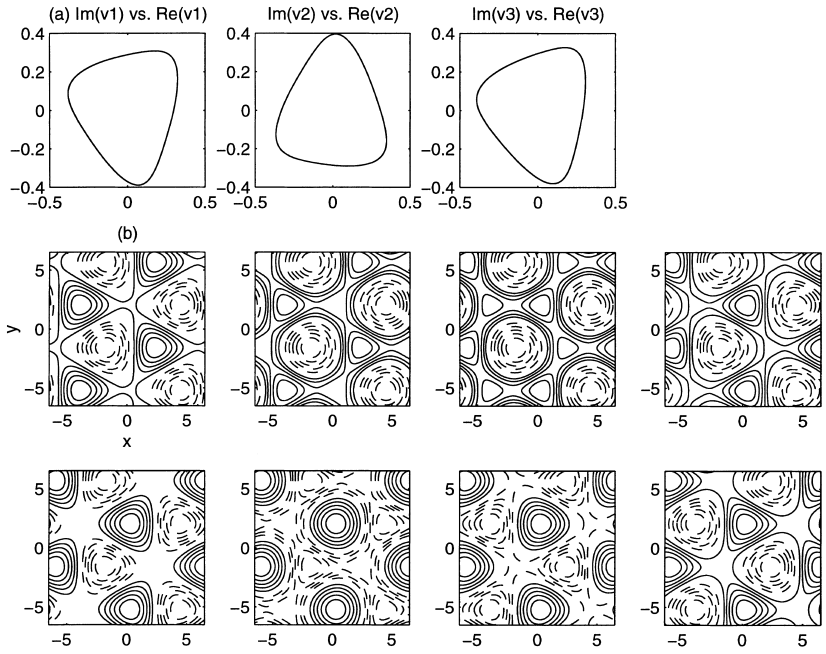

Fig. 23. (a) Temporal evolution of v_1, v_2 and v_3 for Fluorinert/silicone oil, Case (b) of Table 5, and $\epsilon_2 = -2.7$. (b) Spatial evolution for Fluorinert/silicone oil, Case (b) of Table 5, and $\epsilon_2 = -2.7$.

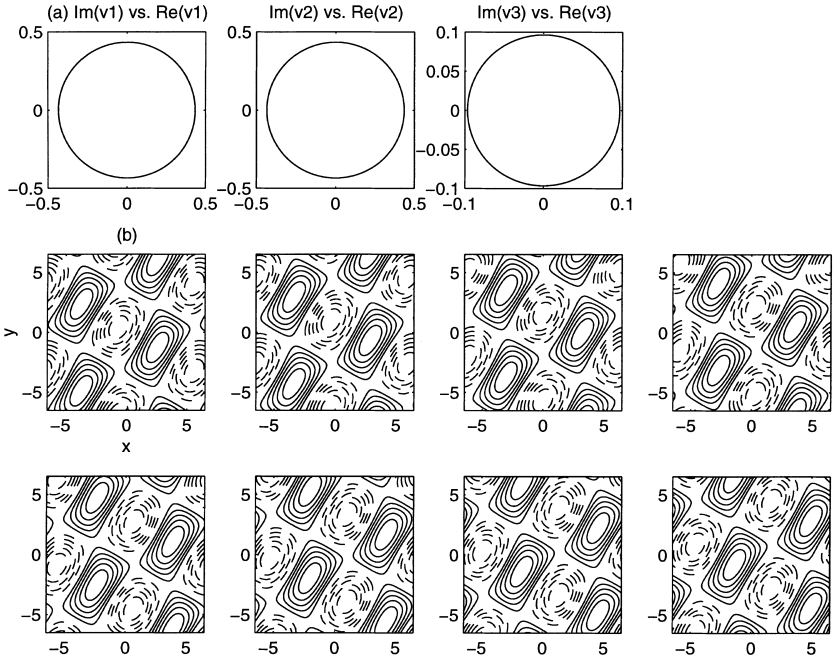

Fig. 24. (a) Temporal evolution of v_1, v_2 and v_3 for Fluorinert/silicone oil, Case (b) of Table 5, and $\epsilon_2 = -3.2$. (b) Spatial evolution for Fluorinert/silicone oil, Case (b) of Table 5, and $\epsilon_2 = -3.2$.

for nearby parameters, suggest that this solution is close to one of the heteroclinic orbits which we investigated in Section 5.5. At $\epsilon = -3.2$, the solution is a traveling patchwork quilt (1).

Case (c), column 1:

The patterns are qualitatively similar to the Anderinert/silicone oil system, Case (a), column 2. We have steady rolls for $\epsilon_2 \geq 2.5$, steady hexagons for $2.4 \geq \epsilon_2 \geq -2.9$, a chaotic regime for $-3.0 \geq \epsilon_2 \geq -3.4$, and wavy rolls (1) for $\epsilon_2 \leq -3.5$.

Case (c), column 2:

In this case, we have steady rolls for $\epsilon_2 \geq 206$, steady hexagons for $205 \geq \epsilon_2 \geq -2.0$, a variety of chaotic and quasiperiodic patterns for $-2.1 \geq \epsilon_2 \geq -7$ (qualitatively similar to Case (a), column 1 patterns), traveling rolls for $-7.5 \geq \epsilon_2 \geq -18$ and wavy rolls (1) for $\epsilon_2 \leq -19$.

7. Conclusion

We have derived the amplitude equations governing the evolution near a Takens–Bogdanov bifurcation with the symmetry of the hexagonal lattice. As in the classical Takens–Bogdanov problem, the leading order approximation is a Hamiltonian system, which is perturbed by dissipative terms at the next order of approximation. We have identified families of periodic solutions of the Hamiltonian system which bifurcate from one of the steady solutions. We have also proved the existence of heteroclinic connections between steady hexagons; these heteroclinic loops represent the limit of a family of periodic solutions ('oscillating triangles'). Numerical integration of the amplitude equations shows that steady solutions (rolls and hexagons) as well as periodic solutions (traveling rolls, wavy rolls (1), oscillating triangles, traveling patchwork quilt (1)) can be observed. The transition from steady to periodic regimes does not occur directly; instead chaotic and quasiperiodic solutions are observed in the intermediate region of parameter space.

Acknowledgements

Y.Y. Renardy acknowledges the support by NSF-CTS9612308. Y.R. and M.R. thank the Japan Atomic Energy Research Institute where this work began during August, 1996. M.R. also acknowledges the support by NSF-DMS9622735 and ONR N00014-92-J-1664.

Appendix A. Coefficients in the amplitude equations

The coefficients in Eqs. (7), (11) and (12) are related as follows. The rest of the coefficients $b_i, c_i, \tilde{b}_i, \tilde{c}_i$ are not required in the analysis of Section 5.

$$b_2 = \frac{(-\beta_1 - \beta_2 - 2\beta_3 + \bar{\beta}_1 + \bar{\beta}_2 + 2\bar{\beta}_3)(\mu - \bar{\mu})}{8},$$

$$b_3 = \frac{\beta_1 - \beta_2 + \bar{\beta}_1 - \bar{\beta}_2}{4},$$

$$c_3 = \frac{\gamma_1 + \gamma_3 - \gamma_4 - \gamma_6 + \bar{\gamma}_1 + \bar{\gamma}_3 - \bar{\gamma}_4 - \bar{\gamma}_6}{4},$$

$$c_4 = \frac{(-\gamma_1-\gamma_2-\gamma_3-\gamma_4-\gamma_5-\gamma_6+\bar\gamma_1+\bar\gamma_2+\bar\gamma_3+\bar\gamma_4+\bar\gamma_5+\bar\gamma_6)(\mu-\bar\mu)}{16},$$

$$c_5 = \frac{-\gamma_1+\gamma_2+\gamma_3-\gamma_4-\gamma_5+\gamma_6-\bar\gamma_1+\bar\gamma_2+\bar\gamma_3-\bar\gamma_4-\bar\gamma_5+\bar\gamma_6}{8},$$

$$c_7 = \frac{(-\gamma_{10}-\gamma_{11}-\gamma_{12}-\gamma_{13}-\gamma_{14}-\gamma_7-\gamma_8-\gamma_9+\bar\gamma_{10}+\bar\gamma_{11}+\bar\gamma_{12}+\bar\gamma_{13}+\bar\gamma_{14}+\bar\gamma_7+\bar\gamma_8+\bar\gamma_9)(\mu-\bar\mu)}{16},$$

$$c_8 = \frac{-\gamma_{10}+\gamma_{11}-\gamma_{12}+\gamma_{13}-\gamma_{14}+\gamma_7-\gamma_8+\gamma_9-\bar\gamma_{10}+\bar\gamma_{11}-\bar\gamma_{12}+\bar\gamma_{13}-\bar\gamma_{14}+\bar\gamma_7-\bar\gamma_8+\bar\gamma_9}{8},$$

$$c_9 = \frac{\gamma_{10}+\gamma_{11}+\gamma_{12}-\gamma_{13}-\gamma_{14}-\gamma_7-\gamma_8+\gamma_9+\bar\gamma_{10}+\bar\gamma_{11}+\bar\gamma_{12}-\bar\gamma_{13}-\bar\gamma_{14}-\bar\gamma_7-\bar\gamma_8+\bar\gamma_9}{8},$$

$$c_{10} = \frac{-\gamma_{10}+\gamma_{11}+\gamma_{12}-\gamma_{13}-\gamma_{14}+\gamma_7+\gamma_8-\gamma_9-\bar\gamma_{10}+\bar\gamma_{11}+\bar\gamma_{12}-\bar\gamma_{13}-\bar\gamma_{14}+\bar\gamma_7+\bar\gamma_8-\bar\gamma_9}{8},$$

$$\tilde b_2 = \frac{\beta_1+\beta_2+2\beta_3+\bar\beta_1+\bar\beta_2+2\bar\beta_3}{4},$$

$$\tilde c_4 = \frac{\gamma_1+\gamma_2+\gamma_3+\gamma_4+\gamma_5+\gamma_6+\bar\gamma_1+\bar\gamma_2+\bar\gamma_3+\bar\gamma_4+\bar\gamma_5+\bar\gamma_6}{8},$$

$$\tilde c_7 = \frac{\gamma_{10}+\gamma_{11}+\gamma_{12}+\gamma_{13}+\gamma_{14}+\gamma_7+\gamma_8+\gamma_9+\bar\gamma_{10}+\bar\gamma_{11}+\bar\gamma_{12}+\bar\gamma_{13}+\bar\gamma_{14}+\bar\gamma_7+\bar\gamma_8+\bar\gamma_9}{8}. \quad \text{(A.1)}$$

References

[1] K. Fujimura, Y. Renardy, The 2:1 steady-Hopf mode interaction in the two-layer Bénard problem, Physica D 85 (1995) 25–65.
[2] M. Renardy, Y. Renardy, Bifurcating solutions at the onset of convection in the Benard problem of two fluids, Physica D 32 (1988) 227–252.
[3] G.Z. Gershuni, E.M. Zhukhovitskii, Convective stability of incompressible fluids, Translated from Russian by D.Lowish, Keter Publishing House, Jerusalem Limited, 1976.
[4] P. Colinet, J.C. Legros, On the Hopf bifurcation occurring in the two-layer Rayleigh–Bénard convective instability, Phys. Fluids 6 (1994) 2631–2639 .
[5] Y. Renardy, Pattern formation for oscillatory bulk-mode competition in a two-layer Bénard problem, Zeitschr. fuer Angew. Math. u. Phy. 47 (1996) 567–590.
[6] Y. Renardy, C.G. Stoltz, Time-dependent pattern formation for two-layer convection, in: M. Golubitsky, D. Luss, S. Strogatz (Eds.), Proc. IMA Workshop on Pattern Formation in Continuous and Coupled Systems, Springer, New York, in press.
[7] F.H. Busse, G. Sommermann, Double-layer convection: a brief review and some recent experimental results, Advances in Multi-Fluid Flows, Proc. of the 1995 AMS-IMS-SIAM Joint Summer Res. Conf. on Multi-Fluid Flows and Interfacial Instabilities, in: Y. Renardy, A.V. Coward, D. Papageorgiou, S.-M. Sun (Eds.), Society for Industrial and Applied Mathematics, 1996, pp. 33–41.
[8] C.D. Andereck, P.W. Colovas, M.M. Degen, Observations of time-dependent behavior in the two-layer Rayleigh–Benard system, paper Da.05, Annual Meeting of the American Physical Society Division of Fluid Dynamics, 19–21 November 1995, also in Advances in Multi-Fluid Flows, Proc. 1995 AMS-IMS-SIAM Joint Summer Res. Conf. on Analysis of Multi-Fluid Flows and Interfacial Instabilities, in: Y. Renardy, A.V. Coward, D. Papageorgiou, S.-M. Sun (Eds.), Society for Industrial and Applied Mathematics, 1996, pp. 3–12.
[9] K.A. Julien, Strong spatial interactions with 1:1 resonance: a three-layer convection problem, Nonlinearity 7 (1995) 1655–1693.
[10] M. Renardy, Hopf bifurcation on the hexagonal lattice with small frequency, Advan. in Diff. Eq. 1 (1996) 283–299.
[11] M.D. Graham, U. Müller, P.H. Steen, Time-periodic convection in Hele–Shaw slots: the diagonal oscillation, Phys. Fluids A 4 (1992) 2382–2393.
[12] E. Knobloch, Oscillatory convection in binary mixtures, Phys. Rev. A 34 (1986) 1538–1549.
[13] J. Guckenheimer, Ph. Holmes, Nonlinear Oscillations, Dynamical Systems and Bifurcations of Vector Fields, Springer, New York, 1983.
[14] J. Guckenheimer, D. Armbruster, S. Kim, Chaotic dynamics in systems with square symmetry, Phys Lett. A 140 (1989) 416–428.
[15] M. Roberts, J.W. Swift, D.H. Wagner, The Hopf bifurcation on a hexagonal lattice, Multiparameter Bifurcation Theory, in: M. Golubitsky, J.M. Guckenheimer (Eds.), AMS Series Contemp. Math., 56 (1986) pp. 283–318.
[16] D.D. Joseph, Y.Y. Renardy, Fundamentals of Two-Fluid Dynamics, Springer, New York, 1993.
[17] S.N. Chow, J. Mallet-Paret, The Fuller index and global Hopf bifurcation, J. Diff. Eq. 29 (1978) 66–85.

[18] Y. Renardy, Errata for [5], Zeitschr. fuer Angew. Math. u. Phys. 48 (1997) 171.
[19] E. Buzano, M. Golubitsky, Bifurcation on the hexagonal lattice and the planar Bénard problem, Phil. Trans. Roy. Soc. London A 308 (1983) 617–667.
[20] S.N. Chow, J.K. Hale, Methods of Bifurcation Theory, Springer, New York, 1982.
[21] G. Dangelmayr, E. Knobloch, The Takens–Bogdanov bifurcation with O(2) symmetry, Phil. Trans. Roy. Soc. London 322 (1987) 243–279.
[22] M. Golubitsky, I. Stewart, D.G. Schaeffer, Singularities and Groups in Bifurcation Theory II, Springer, New York, 1988.
[23] J.C. Alexander, J. Yorke, Global bifurcation of periodic orbits, Am. J. Math. 100 (1978) 263–292.
[24] S. Rasenat, F.H. Busse, I. Rehberg, A theoretical and experimental study of double-layer convection, J. Fluid Mech. 199 (1989) 519–540.